Thresholds and Sediment Transport Dynamics in an Interbedded Shale and Limestone Controlled Urban Watercourse

by

Jeffrey Hirvonen

A thesis
presented to the University of Waterloo
in fulfillment of the
thesis requirement for the degree of
Masters of Applied Science
in
Civil Engineering

Waterloo, Ontario, Canada, 2017

AUTHOR'S DECLARATION

I hereby declare that I am the sole author of this thesis. This is a true copy of the thesis, including any required final revisions, as accepted by my examiners.

I understand that my thesis may be made electronically available to the public.

Abstract

Sediment transport is a fundamental component of research into river morphology and related engineering practices. The relationship between flow and sediment particle entrainment underpins many of the empirical models used to estimate sediment transport dynamics. The scientific literature reports a research gap specific to the thresholds of mobility of different sized particles in non-gravel bed systems, including those in bedrock channels. Particle tracer technology was used to study coarse sediment entrainment and transport dynamics in an urban, bedrock controlled stream channel in Toronto, Ontario, Canada. Passive integrated transponders were inserted in constrained and unconstrained particles within an incised reach of stream. The distribution of particles transport distances conformed to a two-parameter gamma distribution model, which assumes integrations of the travelled series of steps and rests. Size selective dependency of path length was found to increase for coarser clasts, as compared to observed conditions for gravel-bed systems. Coarser particles were also found to transport in an unconstrained mode, as compared to finer grains. A force exceedance model was applied to further test the performance of reported size selective transport relationships for the study site. Many particles were found to transport at critical shear ratios less than 1, when assuming a modified Shields's based model for entrainment. Field data was then used to determine a reference shear based on the smallest magnitude competent storm. The results show that, when compared to alluvial gravel-bed conditions, finer particles require larger thresholds to mobilize and the inverse is true for coarser particles. Using the reference shear conditions, rates of sediment transport were calculated and compared to common models for coarse particle transport. The results confirm size selectivity by grain class and indicate differentiations between fine and coarse transport relationships for the site. This research confirms non-conformity of particle entrainment and transport relationships for the study site, when compared to common empirical model for gravel-bed rivers. The results may be used to obtain critical entrainment parameters and sediment transport relationships, which can then be used to inform design criteria for regional watercourses having like lithology and morphology.

Acknowledgements

I would like to thank my advisor Dr. Bill Annable, for practicing what he preaches in fostering integration between disciplines and for the dissemination of knowledge towards more scientifically defensible and well-rounded approaches to river rehabilitation.

I would also like to thank my research colleagues, whose assistance and encouragement were invaluable in helping to steer this research towards a meaningful end. Special thanks go to Ben Plumb whose willingness to share insight gained from his own research and his generosity of time are forever appreciated. Finally, I would like to thank those who assisted in the collection and analysis of data, including Chris McKie, Terry Ridgeway, Victoria Lounder, Peter Thompson, Jeff Muirhead and Brad Burrows.

Dedication

Dedicated to the memory of my father, who instilled in me a passion for learning and an intellectual curiosity towards environmentally minded pursuits.

Table of Contents

List of Figures

List of Tables

List of Symbols

Symbol	Description
C_d	drag coefficient [-]
d_i	particle diameter of percentile i [L]
d_s	representative particle diameter [L]
d_*	dimensionless particle diameter [-]
d_{mobile}	mean mobile particle size for discrete tracer recovery events [L]
D_{ac}	active depth of the mobile stream bed [L]
g	gravitational acceleration [LT^{-2}]
f_i	ith fraction of the bed material [-]
F_h	particle hiding function [-]
G	specific gravity [-]
k_s	hydraulic roughness [L]
K_G	grain size distribution kurtosis [-]
ℓ_a	particle length of the a axis [L]
ℓ_b	particle length of the b axis [L]
ℓ_c	particle length of the c axis [L]
L_{li}	discrete transport distance for particle i [L]
L'	mean particle travel distance for a 0.5 ϕ grain size class [L]
L'_{D50}	mean particle travel distance of the 0.5 ϕ grain class that contains the d_{50} size [L]
L_{mean}	mean particle path length for discrete tracer recovery events [L]
LC_{mean}	mean path length per particle class size [-]
L_{d50}	mean path length of the particles containing the d_{50} grain size class [L]
N_t	number of total particles recovered [-]
N_m	number of particles found to be mobile [-]
N_{EVB}	number of event-based particles recovered [-]

NC_m	number of seeded particles [-]
p	grain size mixture porosity [-]
PC_m	Percentage of particles found to have mobilized at least once [-]
P_t	percent of all particles recovered [-]
P_m	percent of particles found to be mobile [-]
PC_{mean}	mean particle size for discrete grain size classes [-]
q_{bi}	bedload transport rate [$ML^{-1}T^{-1}$]
q^*_i	dimensionless bedload transport of the ith particle class [-]
q^*	dimensionless bedload transport rate per unit bottom width [-]
Q_i	instantaneous discharge [L^3T^{-1}]
Q_c	critical discharge for threshold of movement [L^3T^{-1}]
R	hydraulic radius [L]
S_b	slope of the channel bed [-]
S_p	particle sphericity (Julien, 1995) [-]
s_a	particle surface area [L^2]
Sk_l	grain size distribution skewness [-]
t	time step [T]
v	kinematic viscosity of water [L^2T^{-1}]
v_b	virtual particle velocity [LT^{-1}]
z_p	height above the bed that is the bottom of the logarithmic velocity profile [L]
V	particle volume [L^3]

Greek symbols

τ_0	channel bed shear stress [$ML^{-1}T^{-2}$]
τ_c	critical shear stress [$ML^{-1}T^{-2}$]
τ_*	dimensionless shear stress (Shields parameter) [-]
$\tau^*{}_c$	critical dimensionless shear stress [-]
τ^*_{ri}	reference dimensionless shear stress [-]
γ	specific weight of water [$ML^{-2}S^{-2}$]
γ_s	specific weight of sediment [$ML^{-2}S^{-2}$]
ρ	mass density of water [ML^{-3}]
ρ_s	mass density of sediment [ML^{-3}]
ϕ	particle angle of repose [-]
ψ	particle sphericity (Wadell, 1935) [-]
Φ	shape specific particle pivoting angle [-]
ω	particle exposure coefficient [-]
σ	particle sorting coefficient [-]

Chapter 1
Introduction

It is generally understood that the overarching suite of processes governing bedrock channel metamorphism differ from those affecting fully alluvial systems (Wohl and Merritt, 2001). High degrees of heterogeneity (Turowski *et al.*, 2008), complex plan and bed form morphology (Goode and Wohl, 2010) and varied lithology (Sklar and Dietrich, 2001) are all contributing factors demonstrated to increase uncertainty in the modelling/prediction of bedrock channel evolution, including those of bed material transport. Snyder *et al.* (2003) characterized the "incision problem" for bedrock systems, which quantifies the stochastic nature of erosion thresholds for these systems and highlights the inherent uncertainty in modelling due to a lack of field data quantifying unknown parameters.

The preponderance of research examining bedrock channel evolution has been focused in upslope mountainous regions. As such, the nature of formative interactions between hydrodynamics, land-use change, geologic conditions and channel morphology is less studied in urban bedrock systems than other channel morphologies. Moreover, channel processes in these settings are more likely to interact with the built environment; thus, this research gap becomes more relevant because of the associated engineering applications. The aim of this research is to study the on-going channel processes of a bedrock channel passing through an urban watershed with nominal stormwater management controls and identify the formative processes and contributing factors to the channel degradation. Sediment mobility parameters arising from these observations are hypothesized to differ from those most commonly reported in the literature for gravel-bed channels, thereby presenting an opportunity to address potential departures in estimating bed material transport in such environments.

1.1 Thesis organization

This thesis follows a manuscript format whereby Chapter 2 provides a broader overview of the study site, Chapter 3 it they body of the manuscript format and Chapter 4 outlines the conclusions and recommendations.

Chapter 2
Study Site Characteristics

Humber Creek (815 ha) is a tributary to the Humber River, in the City of Toronto, Ontario, Canada, that forms part of the Lake Ontario drainage Basin. The effective drainage area is 100 % urban land-use (residential, mixed-used and industrial), that is routed through storm sewers to the creek (City of Toronto, 1999). The headwater drainage system is a storm sewer network draining industrial lands east of Pearson International Airport. The stream network is divided into two distinct morphological units delineated by the degree of incision and floodplain connectivity (Figure 1). Station (STA) references are defined from the downstream confluence with Humber River (0+000) to 4+070 at the upstream limit of open channel. Approximately 78% (3170 m) of the watercourse has access to the floodplain during some part of the typical annual flow regime.

Urbanization progressed across the watershed predominantly during the mid-20th century, with its entirety urbanized by the late 1960's. During this period, natural drainage pathways were replaced by storm sewer networks with few engineered stormwater management controls as development predated most stormwater management best practices. At approximately STA 0+900, the watercourse transitions into a deeply incised reach with interbedded layers of shale and limestone (forming part of the upper Ordovician Blue Mountain bedrock formation (Watt, 1966)) which persists to its confluence (STA 0+000). Vertically, this transition is artificially maintained by a grade control structure covering a sanitary sewer crossing preventing knickpoint migration. Bank height increases in this reach by a factor of 10 and becomes fully disconnect from its floodplain (no major increase in width-to-depth ratio for any storm magnitude up to the 1:100 return interval event). Channel form is maintained by channel bottom and bank materials consisting of the weathered shale and limestone.

There is a notable grade separation at Scarlet Road (Figure 1b) produced by the introduction of a culvert in 1954. The culvert invert on the upstream side of the road maintains the thalweg grade of the lower limit of the incised channel whereas a 3m vertical drop occurs on the downstream side of the culvert which then transitions to its confluence with Humber Creek. This research focuses on the 1200 m reach of incised channel upstream of Scarlett Road.

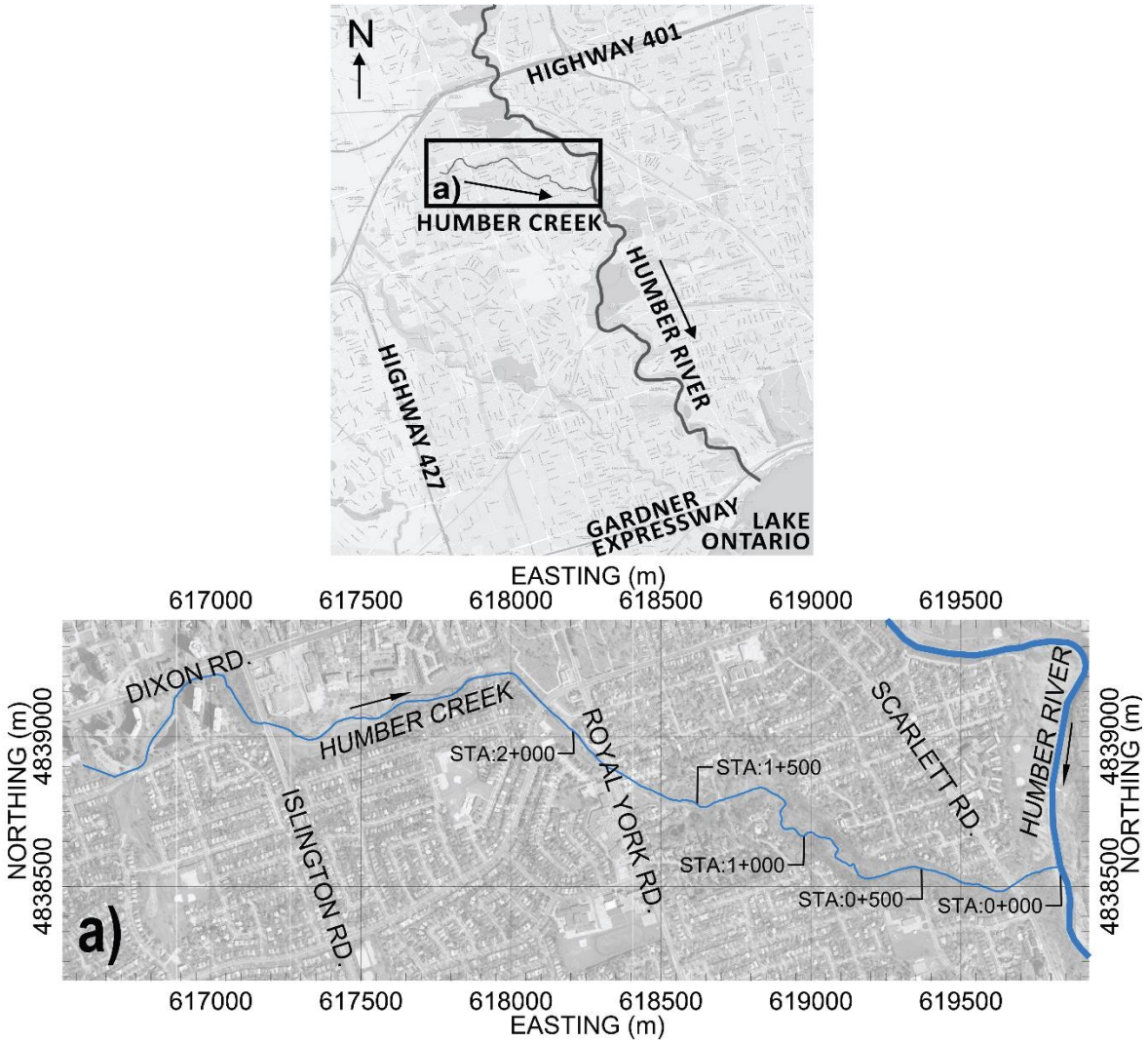

Figure 1 – Humber Creek site location and a) daylighted Humber Creek Reach. Sources: Toronto and Region Conservation, ESRI, City of Toronto (2009 base mapping)

Some representative photos have been included below to illustrate the nature of bedform complexity at the study site. Photo Plate 1 illustrates the complex planform morphology, in this case caused bed an erosion resistant bedrock outcrop. This type of abrupt transition occurs in plan and profile, typically occurring at the interface between different geologic horizons or at geologic fault lines.

Photo Plate 2 shows an example of exposed bedrock on the channel bottom, which follows a more complex series of imbricated bed forms immediately upstream. There are a number instanced where similar bed form sequences (having a high degree of heterogeneity) exist close proximity to one another.

Photo Plate 1 – Example of complex planform morphology at the study site.

Photo Plate 3 illustrates an example of coarse particle imbrication, in this case positioned immediately adjacent to an unconstrained section of exposed bedrock on the channel bottom.

Photo Plate 2 – Example of unconstrained bedrock channel bottom (foreground) and more heterogenous bed forms (background).

Photo Plate 3 – Example of plan and profile complexity. Imbricated coarse particles (circled) sit adjacent to an exposed bedrock bed.

.

Chapter 3
Coarse Sediment Transport Processes in an Urban Bedrock System

3.1 Introduction

Bedload transport rates and mechanisms of coarse sediment are known to govern rates of morphological change in natural watercourses (Leopold, 1994; Jackson and Beschta, 1984). Research into bedload transport dynamics has quantified the mobility of different grain size distributions in flumes (Shields, 1936; Wilcock, 1993) and in natural watercourses, with most field research focusing on rural, sand and gravel-bed rivers. Several models and empirical relationships have been developed for different classes of rivers and grain sizes, mostly for sand and gravel dominated systems, including single grain entrainment models (e.g. Shields, 1936) and fractional transport models (Parker, 1990; Wilcock and Crowe, 2003). It is also known that gravel-bed particles have threshold conditions (Komar and Li, 1986) and transport dynamics (Goode and Wohl, 2010) that differ from more angular and platy particles that are characteristic of the bedrock governing the study site.

Wohl and Merritt (2001) investigated an overarching set of processes governing bedrock channel morphologies, and concluded that they differ from those affecting fully alluvial systems. Several extraneous factors beyond channel hydraulics are known to contribute to bed material supply such as rock strength, antecedent weathering processes, chemical weathering, etc. (Sklar and Dietrich, 2001). Once detached by mechanisms such as plucking and cavitation, bedrock clasts typically have greater angularity than do alluvial particles weathered by fluvial forces (Whipple *et al.*, 2000). Inherent differences in the relationship between particle shape and entrainment are dependent on angularity (Julien, 1995; Komar and Li, 1986), and the arrangement of coarse particles (e.g., mode of imbrication) which have also been identified to effect particle mobility (Lamarre and Roy, 2008). Bedform roughness, which may also increase due to coarse particle clustering arrangements, is an further confounding factor for sediment transport processes (Goode and Wohl, 2010) and has been found to be underrepresented as a resistance factor in predicting bedload transport rates (Chiari and Rickenmann, 2007; Schneider *et al.*, 2015).

In urban river systems, hydromodification caused by urbanization affects sediment transport dynamics in terms of bed material supply, bedload transport rates and sediment grain size fractions (Lisle and Madej, 1992; Pizzuto *et al*., 2000; Annable *et al.*, 2012). The effects on urban channel morphology have been studied with respect to modes and mechanisms of change, including channel incision as a primary response to urbanization (Booth, 1990), but have been less studied in terms of in-situ bedload transport for discrete urban hydrological settings. Some studies have been conducted in gravel-bed rivers, where

the role of coarse particle mobility has been shown to influence the arrangement of bed forms and, ultimately, the dissipation of energy (Hassan *et al.*, 2008). Few studies have investigated the transport dynamics of discrete bedload particles in non-gravel bed systems.

This study addresses a research gap specific to the transport dynamics of coarse sediment in urban, bedrock systems. It is hypothesized that the transport of discrete coarse particles in bedrock systems differs from results observed in alluvial systems. This hypothesis has relevance to engineering problems in remedial channel works because of the many bedload transport models and parameters that can be applied in the assessment and prescription of channel processes that assume fundamental values derived from gravel-bed channel (or similar, for laboratory settings) settings. Here, a field program was undertaken to track discrete particles and to relate the modes and rates of transport to hydraulic forces acting on the channel boundary in an urban bedrock channel environment. The study examined several hydrological events and compared the relevant transport distances, particles sizes and transport between geomorphic units to modelled hydraulic forces known to influence particle mobility.

3.2 Background

3.2.1 Bedrock Morphology and Transport of Bedrock Sediment

Wohl (1998) describes bedrock erosional processes whereby the resistance of the channel substrate overwhelmingly dominates the morphology and rate of channel adjustment, and points to rock resistance factors such as intact strength, porosity, permeability and heterogeneity (both from a macro and micro scale) as playing roles in determining mechanisms of change in bedrock morphology. That change is subject to an overarching set of processes acting to erode bedrock channels, including: dissolution, plucking and cavitation (Whipple *et al.*, 2000), freezing and thawing (Robinson *et al.*, 2001) and impact erosion (abrasion) (Sklar and Dietrich, 2001). In addition, local bedrock terraces and faults have also been known to significantly influence bedrock morphology and rates of erosion (Buffington, 2004). The relationships between driving and resisting forces are illustrated in Figure 2.

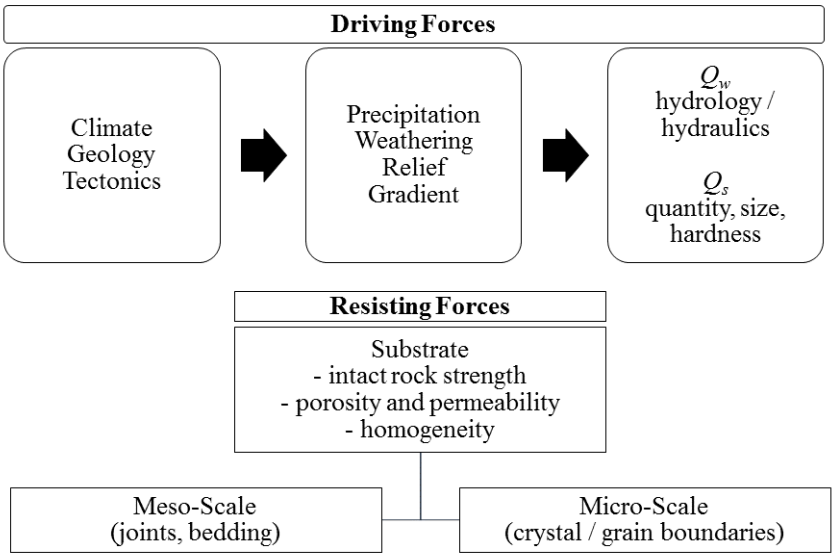

Figure 2 - Bedrock channel processes - driving versus resisting forces in determining channel forming processes (reproduced from Wohl, 1998)

In cases where bedrock sidewalls are present and resistant to erosion, the dominant mode of channel adjustment is channel incision and stochastic knickpoint propagation, resulting in the formations of steps caused by episodic and alternating instances of erosion and deposition (Schumm *et al.*, 1984). Knickpoint propagation in bedrock systems, while having the same equilibrium-driven mechanisms as alluvial

channels, operates in a much more stochastic nature due to the higher degree of influence by bed form complexity (Goode and Wohl, 2010) and particle interactions (Wohl, 1998).

Intuitively, one of the primary differences between alluvial and bedrock systems is the derivation of sediment from its source in that, depending on the nature of the lithology, increases in velocity and shear stress may not result in corresponding particle detachment rates. Several factors extraneous to the channel hydraulics combine to establish the availability of sediment (Sklar and Dietrich, 2001). For example, some antecedent substrate conditions contrasting alluvial channels and factoring into sediment supply which include: rock type(s); meso scale fault lines and fissures; micro scale crystal formation and fissures; geologic stratification; freezing and thawing cycles and wetting and drying cycles (Tinkler and Wohl, 1998).

Mass wasting, or the geotechnical failure of large clasts in the case of bedrock channels, is one common mechanism of particle detachment (Robinson *et al.*, 2001). However, the mode of failure may or may not be influenced by the flow regime of the channel. Also, the transition from particle detachment to particle transport is not linear, resulting in scaling challenges when trying to apply regional relationships for predicting bedrock channel morphology, which can vary widely due to climatic conditions (Wohl and David, 2008; Viles, 2001).

Once detached, the entrainment and transport of individual clasts are represented by the conservation of momentum and subject to applied hydraulic boundary forces. Goode and Whol (2010), however, observed that after the point of incipient motion, sediment transport dynamics within bedrock systems are influenced by factors that contrast many alluvial systems, including inherently low sediment loading rates, highly turbulent conditions capable of transporting very large particles and hillslope connections that supply coarse sediment through diffusive processes. Goode and Whol also point to the effect of bed form roughness generated by the sculpted nature of bedrock channels, and theorize that this inherently increases form drag and reduces bed shear, thus reducing local sediment transport rates and increasing the role of bedrock topography on spatial distribution of sediment transport.

All of these factors combine to create complex interactions between geology, climate and hydrology as the state variables governing morphology and sediment transport in bedrock systems. By combining a review of the literature and the characteristics of the study site being researched (with local conditions described in Chaper 2), Table 1 lists contributing factors that may play a role in the evolution of bedrock channels

Table 1 – Modes and mechanisms of particle detachment and entrainment pertinent for the Humber Creek study reach.

Mode	Mechanism	Description
Weathering / Detachment	Free-thaw / wetting-drying	Repeated cycles of wetting, drying, freezing and thawing that cause fracturing and desiccation of shale and limestone.
	Chemical dissolution	Calcite dissolution and micro/ macro joint expansion by groundwater.
	Cavitation	Failure by gravity of weathered bedrock. Typically occurs on channel banks and at high overflow areas. This process is often accompanied by anteceded weathering related to the modes above.
	Scour	The persistent removal of small pieces of bedrock (in the case of Humber Creek shale) by jet scour, typically at an overflow. Process is continual as a function of scour jet hydraulics.
	Plucking / Mining	The removal by hydraulic forces of fractured or weathered bedrock clasts from the bed. Typically preceded by weathering processes which expand micro fissures into macro joints. Process is episodic.
	Tool and cover effect	Effect of thin layer of alluvium overlying bedrock bed. The thickness and spatial distribution of this layer controls the degree to which particle collision can generate fractures of the bed material and act as the catalyst for further particle detachment.
Entrainment / Transport	Collision	Degree to which momentum transfer by coarse particle collisions affects rates of sediment transport.
	Tractive Force	Incipient motion and transport of detached particles by shear forces.
	Particle interactions	Particle hiding, imbrication, clustering, layering and other arrangement of particles.
	Bedforms	Persistent macro forms (either formed by particles or geology) that affect local sediment transport by forcing flows.

3.2.2 Particle Threshold Hydrodynamic Mobility and Sediment Transport

Quantification of vertical bed stability within a watercourse is defined by the system's inherent ability to resupply particles mobilized from the bed. Once physical detachment of the substate and bank material occurs, it is required that there be sufficient force within the watercourse to transport the partcles downstream, otherwise an imbalance occurs and the system is said to be unstable (Makin, 1948). The entrainment and transport of individual particles and bedrock clasts can be represented by the conservation of energy, whereby impelling forces exerted by the downslope component of the weight of water are resisted by a counteracting force, primary shear stress. The average boundary shear stress is expressed as:

$$\tau_0 = \gamma R S_b \tag{1}$$

where τ_0 is the channel bed shear stress ($ML^{-1}T^{-2}$), γ is the specific weight of water ($ML^{-2}S^{-2}$), R is the hydraulic radius (L) and S_b is the bed slope (-).

Specific to the forces acting on individual particles, an excess shear stress model may be applied. Shields (1936) used empirical data for individual grain sizes to develop a dimensionless form of the shear stress equation defined by the ratio of downstream drag force acting on the bed (τ_0) to the weight of the submerged particle as:

$$\tau_* = \tau_0/(\rho - \rho_w) g d_s \tag{2}$$

where τ^* is the dimensionless shear stress (the Shields parameter), ρ_s is the sediment density (ML^3), ρ_w is the water density (ML^{-3}), g is gravitational acceleration (LT^{-2}) and d_s is the characteristic particle diameter (L). For critical values of τ^* Julien (2002) demonstrates that at the point of incipient motion ($\tau_0 = \tau_c$, where τ_c is the critical bed shear stress) a critical shear value ($\tau^*{}_c$) can be calculated via the intersection of the Shields parameter plot (for a variety of grain size ratios), with the dimensionless particle diameter (d_*), expressed as:

$$d_* = d_i \left[\frac{(G-1)g}{v^2}\right]^{1/3} \tag{3}$$

where d_i is the particle size, G is the specific gravity of the sediment (-) and v_m is the kinematic viscosity of the mixture (L^2T^{-1}). $\tau^*{}_c$ is otherwise referred to hereafter as the modified-Shields method (or

diagram) which can also be used as comparative measure of common threshold applications in engineering practice for a given grainsize diameter d_i.

Other empirical research into the threshold of motion for particles has focused on velocity as the determinant for mobility (Komar, 1987), or on the flow velocity required to maintain transport of a particle already in motion. This is an important point in understanding the conceptual difference between sediment transport and incipient motion. Incipient motion describes the point at which a particle d_i begins to move under a given applied force, whereby the resistance to incipient motion is most affected by the weight of the particle and its angularity (Julien, 1995), whereby the angle of repose (ϕ) of a given particle is a function of the particle angularity. In laboratory studies, Buffington *et al.* (1992) and Li and Komar (1986) quantified the friction angle required to mobilize particles of different shapes, while Carling *et al.* (1992) studied transport modes and rates for different shapes. Siddiqui and Robert (2010) studied particle mobility in similar lithology in Southern Ontario, including an examination of flow over imbricated particles in a flute. In each study, particle shape and degree of imbrication was found to be significant factors in determining both the threshold for motion and the mode and rate of transport.

It is then reasoned that the inherent shape of bedrock substrate may result in incipient conditions and rates of transport that differ from rounded gravel-bed material, which make up the basis for most field-driven experiments testing particle transport models. This hypothesis agrees with experiments by Ashworth and Ferguson (1989) who found correlations between particle sphericity and transport distance, evidenced by spherical particles being transported larger distances than angular ones. This also agrees with the work of Komar and Li (1986), who augmented their laboratory findings with excess shear stress models specific to different particles shapes.

Critical threshold estimates are important metrics to a class of sediment transport model that considers excess applied force greater than that required to initiate incipient motion. Parker *et al.* (1982) describe a reference condition, which is a method for estimating the threshold condition. The concept of reference shear is well studied (Parker *et al.*,1982; Wilcock, 1993), and uses an empirically derived threshold of mobility to define a small amount of shear stress that generates minimal transport of a given grain size fraction. Reference shear conditions have been derived from laboratory flume studies (Shields, 1936; Li and Komar, 1986; Wilcock, 1993) or from field data using trapped, traced or in situ bedload sampling techniques (Ashworth and Ferguson, 1989; Parker *et al.*, 1982; Wathen, *et al.*, 1995). In place of absent field data identifying the hydrodynamic thresholds of incipient motion for a given representative grain diameter, the most common approaches are to employ empirical relationships developed by others. Shields (1936) particle mobility diagram for example (or variants thereof) is a commonly applied method.

The bulk rate of sediment transport once entrainment is commonly estimated from one or more empirical formulae commonly derived from laboratory experiments or from a sparse suite of field data sites. Various examinations of these formulae have demonstrated orders of magnitude in degrees of predictive variability for gravel-bed rivers (e.g. Gomez & Church, 1989). This uncertainty notwithstanding, the estimation of bedload transport rates remains relevant to engineering applications such as drainage canal design, aggregate extraction from rivers, dam assessment and design and linear infrastructure (e.g. bridge and pipeline) scour protection and habitat rehabilitation (Parker, 2006).

Gomez and Church (1989) group the most common sediment transport models based on their constituent parameters describing sediment mobility, including those based on stream power models, tractive force (including excess shear stress) and a third subset considered to have common parameter groupings employed by a specific research group. The tractive force group has the most direct relevant to the current study site, owing to the availability of a detailed hydraulic model and hydrology data, and to sediment entrainment data from the tracer study. Suitable model selection and application from within this empirical subset is specific to the study site parameters (see Methods section for this study). Tracer Particle Research, Including Passive Integrated Transponders (PIT Tags)

3.2.3 Tracer Particle Research, Including Passive Integrated Transponders (PIT Tags)

Following the onset of incipient motion, the transport of particles through a system is known to occur by a series of stochastic steps and rests driven by applied fluvial forces, resisting (particle specific) gravitational forces and particle interactions (Einstein, 1950). For this reason, researchers study the movement of discrete particles that are assumed to have traveled through step and rest periods, such that the effects of unconstrained forces and particle interactions are inherently captured by the travel distances.

Researchers have historically used a variety of tracer methods to measure the dispersion and transport of individual coarse particles transported in river systems. Methods have included painted clasts (Laronne and Cason, 1976) or magnetic (Ferguson and Wathen, 1998) markers. These methods often yielded poor recovery rates of tagged particles for reasons such as abrasion and the sorting that occurs naturally in river systems (Lamarre *et al.*, 2005).

Lamarre *et al.* (2005) describes recent methods for seeding coarse particles with 23 mm long glass-encapsulated Passive Integrated Transponder (PIT) tags embedded within the particles themselves. A PIT tags is encoded with a unique digital identifier corresponding to a specific particle. An open loop inductor antenna is used to generate an electromagnetic field and receive the particle ID number. Houbrechts (2012) highlighted the limitations of minimum particle size imposed by the PIT tag seeding technology

and methods, which biases the data towards coarser particles and under represents the finer fraction of the bed material load.

Commonly, tracer experiments have focused on the relationships between particle transport distance and either particle size or the forces applied by the flow. Size selectivity is typically analyzed with respect to particle size classes, with the Wentworth scale being a common size class differentiation method (Bunte & Abt, 2001). This system commonly expresses particle size units as mm or ϕ, with the latter being the negative base-2 logarithm of the particle size (Krumbein, 1941), for achieving a normally distributed population of particle sizes

Ashworth and Ferguson (1989) used in-situ bedload sampling data and dimensionless bedload transport relationships to investigate size selectivity of particle transport to validate assumptions regarding the stochastic nature of coarse particle transport (and to see if observations agreed with the threshold calculations). They found that the tracer experiments supported the threshold estimations from the shear stress and bedload sampling; namely the importance of relative grain size to incipient motion, as compared to absolute grain size.

Church and Hassan (1992) completed several studies using tracer particles on a gravel-bed stream in British Columbia. Their work examined relationships between particle mobility (path length), particle size and applied shear stress, with an emphasis on fractional entrainment and transport. Their results revealed a decreased sensitivity of smaller particles to transport distance, owing to the effect of 'hiding' in the void spaces of larger particles. The excess shear stress models shed light on the non-linearity problem of fractional transport estimations where they found large fluctuations (order of magnitude) in shear stresses required to initiate motion, in addition to a high degree of disparity between observed results and those threshold conditions predicted by flume experiments.

Bradley and Tucker (2012) employed PIT tag tracer technology to compare the mobility of particles to stochastic random walk models that predict intermittent and short duration particle transport distances between long rest periods. Their results suggested that a gamma distribution function best approximates the observed distribution of travel path lengths, in particular for mobility during high flow events. The relationship was weaker for low flow events yielding shorter path lengths.

PIT tag based studies have also been completed in steeper systems, having coarser median particle sizes and more complex morphology analogous to step pool channel bottom profiles. MacVicar and Roy (2011) seeded a short reach of Moras Creek (bed slope = 0.012 m/m) to investigate the transport of coarse particles through a forced riffle-pool morphology. The objective of this research was to gain an

understanding of sediment transport processes in systems transitioning between plane-bed morphology and complex riffle pool structures. They used PIT tag technology to track mobile particles and compare their path lengths to the spatial distribution of shear stress, turbulent kinetic energy (TKE) and resulting changes in bed morphology derived from the competent events. Results indicated a good correlation between critical shear exceedance and particle mobility, with 70% of particles subject to excess shear stress having been mobilized. Results also showed a bias towards coarser particle mobilization (those closer to the d_{84} percentile) and its correlation to average shear stress, as compared to the TKE analysis which was observed to be biased towards the median particle size.

3.3 Methods

3.3.1 Field Program

The study reach is shown in Figure 3. The field program included a geomorphologic assessment, streamflow gauging, and a particle tracer study. Sediment transport related research components were timed to coincide with flashy convective storms.

A morphometric survey (Harrelson *et al.*, 1994) was completed using a combination of Real Time Kinetic (RTK), survey – grade GPS and Total Station Survey having approximately ±2 cm vertical and horizontal accuracy (Sokkia Corporation, 2011) to capture the bed, bank and valley topography. Surveyed morphological parameters in the longitudinal direction included channel centreline, thalweg, bankfull stage indicators, knickpoints, headcuts, bar formations, and instances of the watercourse interfacing with civil infrastructure following the methods of Annable (1996). Centreline and thalweg observations were longitudinally spaced on average at one channel bottom width (5 m), with actual spacing much closer owing to the complex bed morphology. The bedrock channel side walls were surveyed from bottom to top of bank, to facilitate cutting of cross section transects (at the desktop) anywhere within the study reach, for modelling purposes.

Diagnostic substrate sampling was undertaken following the methods of Wolman (1954). Based on initial site reconnaissance, it was determined that the general substrate composition is coarse in nature (few particles smaller than cobble) and has little to no vertical stratification. Particles are either singularly deposited over bedrock, or mixed into heterogeneous bedforms lacking in uniform periodicity or structure. Selected particles were measured along their a-, b- and c- planes in order to quantify the particle size and shape. To capture a broad range of particles spanning different morphologies and sub-reaches, four sample sites were selected (Figure 3), with each being located either at riffle or run regions. The

longitudinal profile is also shown, including the location of a notable headcut. Sub-reach averaged parameters are listed in Table 2.

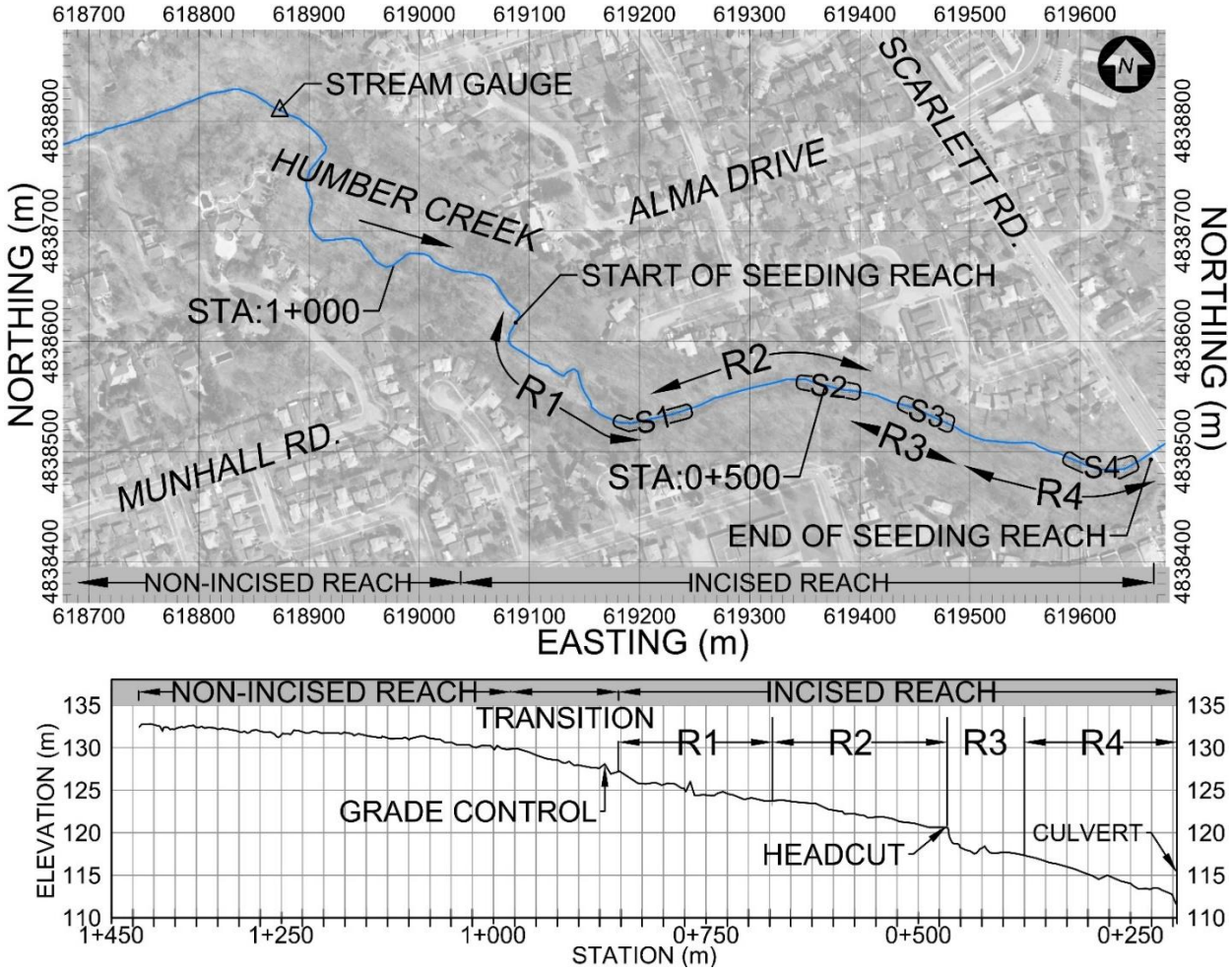

Figure 3 – Humber Creek study reach planform (UTM Zone 17N grid) and profile. Substrate sample Sites S1 to S4 numbered. Geomorphic sub-reaches R1 to R4 within the incised reach shown on plan and profile.

Table 2 – Humber Creek sub-reach delineations and associated and geomorphic parameters. Upstream limit (river station 850.00) corresponds to beginning of incised, bedrock portion of Humber Creek. Downstream limit (river station 201.24) corresponds with Scarlett Road culvert inlet.

Average	**Sub-Reach ID**			
Hydromorphic Parameters	**1**	**2**	**3**	**4**
Upstream Boundary (River Station)	850.00	671.66	466.78	377.01
Downstream Boundary (River Station)	671.66	466.78	377.01	201.24
Bed slope (m/m)	0.018	0.014	0.036	0.022
Width (m)*	7.67	8.82	5.14	9.70
D_{50} grain size (mm)	25.72	20.64	n/a	94.05
Manning's n	0.034	0.032	0.030	0.042

*as defined by bedrock side wall

Clusters of substrate were also seeded with 250 passive inductive transponder (PIT) tags, drilled into bed material particles of differing sizes, having minimum, mean and maximum b-axis dimensions of, 25 mm, 287 mm and 1000 mm, respectively. The seeding program was restricted to the upper 400 m of the incised reach to allow for sufficient distance (265 m) between the downstream most seeded particle and study limit. This also positioned the seeding zone upstream of a morphologically distinct headcut, which would allow for the subsequent analysis to consider transport mechanisms through this feature. The location of seeded particles are shown in Figure 4.

PIT tagged particles were measured for a, b and c axis dimensions and photographed with reference scales. Installation involved drilling of selected particles with a hole to house a 23 mm long, 4mm diameter glass encased PIT tag (134.2 kHz), and then filling the hole with an epoxy resin. In order that the particles could be drilled without causing desiccation or fracturing of the stone, a minimum particle size of 25 mm (b axis) was used during instrumentation, highlighting the challenges with this technology observed by others (Allan *et al.*, 2003; Lamarre *et al.*, 2005, MacVicar *et al.*, 2015).

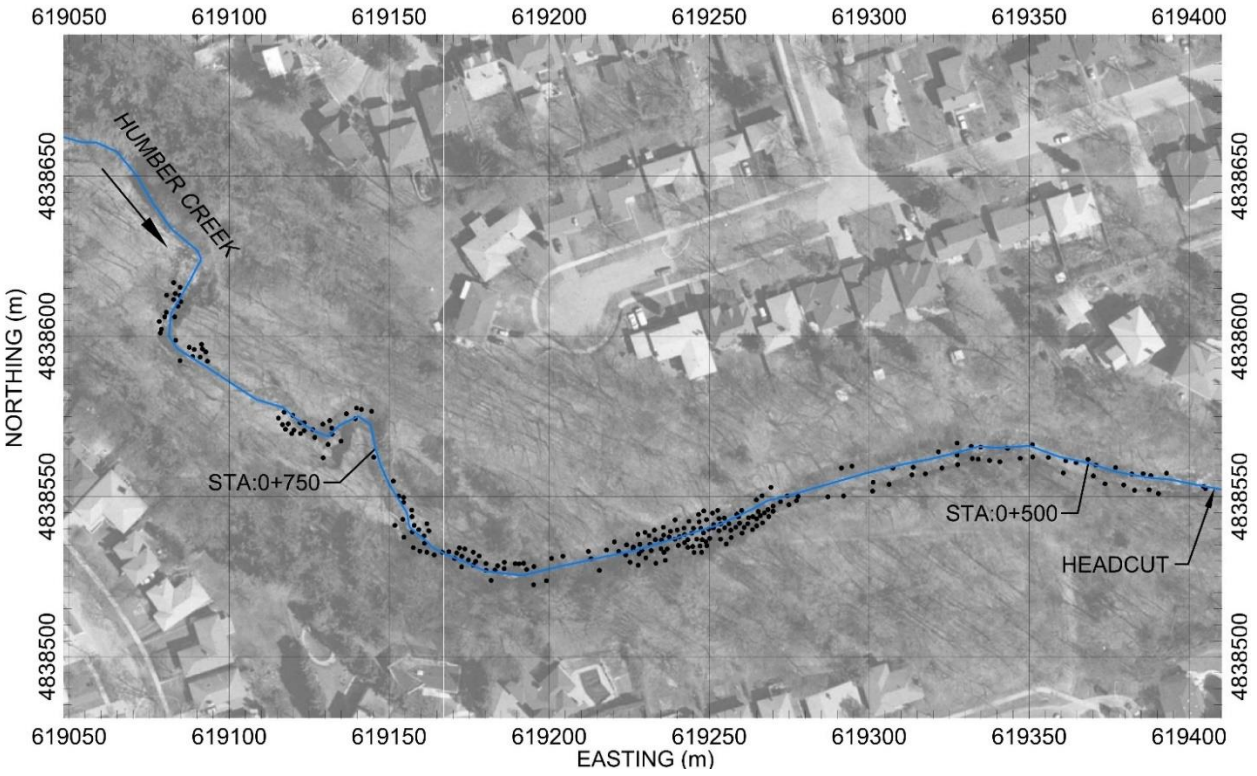

Figure 4 - Spatial distribution of particles seeded with PIT tags (black dots) in Humber Creek. 50 m grid lines shown.

The particles were then replaced on the creek bed in their pre-disturbed position. Each particle was subsequently surveyed by total station and its PIT tag ID number recorded. The nature of the bed material in Humber Creek is such that most of the particles selected for PIT tagging were not naturally embedded, and thus could be replaced following tagging in a location and position mimicking the undisturbed condition.

The reach was seeded in July 2010, after which several small to moderately sized storms occurred in hopes that seeded particles would reintegrate with the natural substrate. Following this, a series of particle recovery surveys were undertaken following major storm events between the period of October 2, 2010 and March 25, 2012. Tagged particles were located using an Aquartis Leone 0.5 m loop wand type reader (Aquartis, 2011) without disturbing their natural position on the creek bottom. A total of seven particle tracking surveys were completed during this period.

The locations of individual particles were subsequently mapped with respect to the longitudinal centreline chainage, which served as the reference distance for all analyses that required particle location and travel distance. Each mapping node contained attributes identifying the location, size and shape of

each specific particle. To assess the number of particles found to be mobile, each event was compared with the preceding recovery results, and particles were identified as either 'paired' or 'unpaired', with pairing referring to particles that were found to be mobile in successive recovery events (Schneider *et al.*, 2014), termed N_{EVB} for event-based recovery. The percent of particles found to be mobile (P_m) is a function of $(N_m/N_{EVB})\times 100$, where N_{EVB} is the total number of event-based paired particles that moved.

3.3.1.1 Streamflow Measurements

The creek was instrumented with Water level logger (Onset (Hobo) model U20-001-01) 360 m upstream of the incised study reach (Figure 3) with a three-minute sampling frequency. The site was also instrumented with two survey control bars in the floodplain adjacent to the gauge to verify if at-a-station changes occurred due to channel incision or deposition during the period of rating curve development. No change was observed.

14 streamflow measurements were conducted at varying water surface stages using a manual acoustic Doppler velocimeter (ADV). Measurements occurred between September 21, 2009 and June 1, 2012 which spanned the entirety of the safe wadable portion of the cross-section. The corresponding streamflow was estimated using the velocity–area method (Rantz, 1982). The measured flow depths ranged between 0.03 m and 0.75 m (approximately ¾ the bankfull depth), having discharge values ranging between 0.009 m^3/s and 5.785 m^3/s and resulting in the at-a-station rating curve (Figure 5).

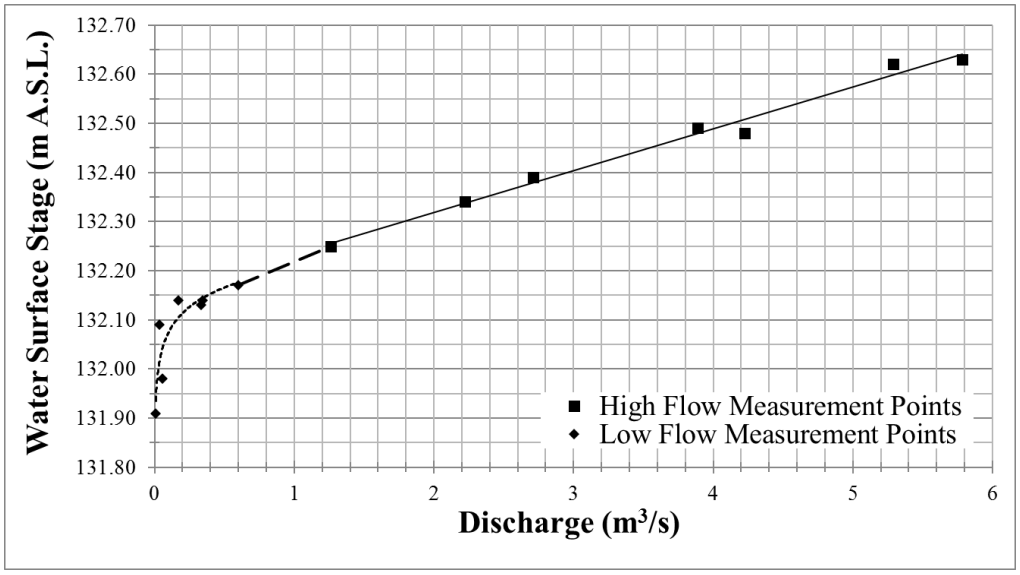

Figure 5 – Stage-discharge plot for the Humber Creek stream gauge site. Low flow discharge power fit represented by short dashed line, high flow linear fit by solid line. Interpolated long dash linear fit between low and high discharge measurements.

The stage-discharge relationship was then applied to the pressure transducer data, adjusted for barometric pressure, and a time series data set derived (Figure 6). Two events exceeding bankfull were noted to have occurred. Unfortunately, a malfunction within the pressure transducer resulted in errors for a portion of the data record. The corrupted data set was limited to dates encompassing the first two post-seeding PIT tag tracking surveys, thus limiting the hydrodynamic and sediment transport study to the latter three tracking surveys.

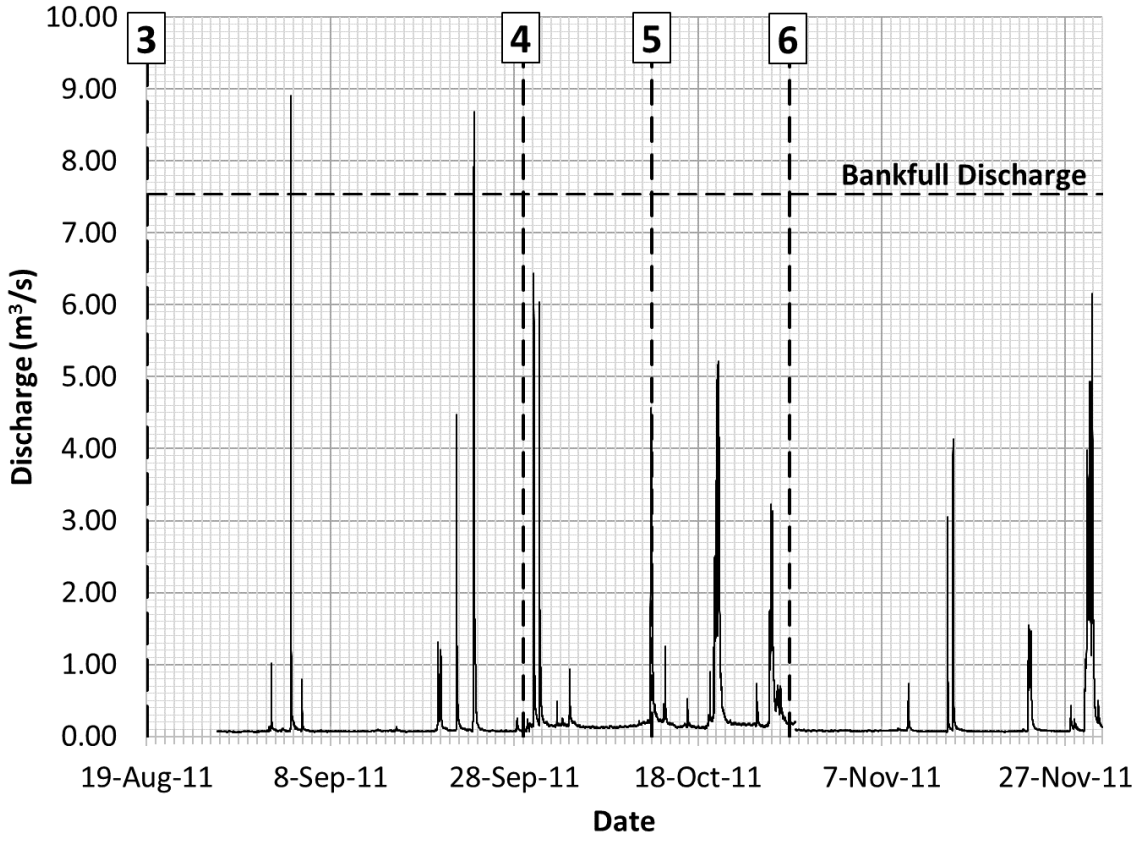

Figure 6 - Humber Creek flow record between August 26, 2011 and December 1, 2011. Bankfull discharge plotted as dashed line. Tracer recovery events shown as dashed vertical lines and labels.

3.3.2 Substrate Analysis

436 particles were inventoried with PIT tags and a grain size analysis conducted for both data sets. Data set 1 included four pebble counts that randomly sampled from all bed material in the study reach. Data set 2 included only PIT tag seeded particles. The two data sets were kept separate to maintain the random

quality of Data set 1, due to Data set 2 being less random (owing to challenges securing PIT tags within smaller particles). For each data set, grain size parameters were determined including: particle surface area calculated from axis lengths; the particle surface area measured from photogrammetry; the particle volume and associated mass (based on assumed mass density of the material); and, the particle sphericity and shape classification.

Grain size distributions were plotted for cumulative frequency distribution (Bunte and Abt, 2001) for each sampling site shown in Figure 3, and an aggregate of all samples, with distributions plotted in Figure 7. All samples indicate a dominance of coarse substrate, with a general trend towards increased particle size in the downstream direction. The d_{50} ranged between 20 and 90 mm, with an aggregated d_{50} = 34.19 mm. Sample 1 is slightly finer in the upper percentiles and Sample 4 is coarser in the lower percentiles. A distinct coarser fraction is observed in Sample 4 for the 70% percentile and finer range. This sample is in a sub-reach upstream of the Scarlett Road culvert crossing where a depositional feature exists likely resulting in the coarser distribution. Intermediate (b) axis values were then tallied and binned into 0.5ϕ grain size intervals. Size classifications were determined as per the Wentworth scale (Wentworth, 1922). Table 3 lists basic grain size characteristics for different fractions in addition to basic descriptive statistics, as per Folk and Ward (1957). In Samples 2 and 3, skewness values show the distribution is biased towards the finer fractions, while the opposite is true for Samples 1 and 4. The divide between distribution kurtosis is also found in Samples 2/3 and 1/4, with the former plotting to be flat or not especially peaked, and the latter as highly peaked (Folk and Ward, 1957). The morphology includes intermittent areas of exposed bedrock which, based on the results, are most prevalent in the two reaches immediately upstream of the headcut (located at STN 0+464). For the aggregated values, $Sk_l = 0.21$ indicates a slight skew towards the finer grain size fractions and $K_G = 1.01$ indicates the sample follows a normal degree of peakedness.

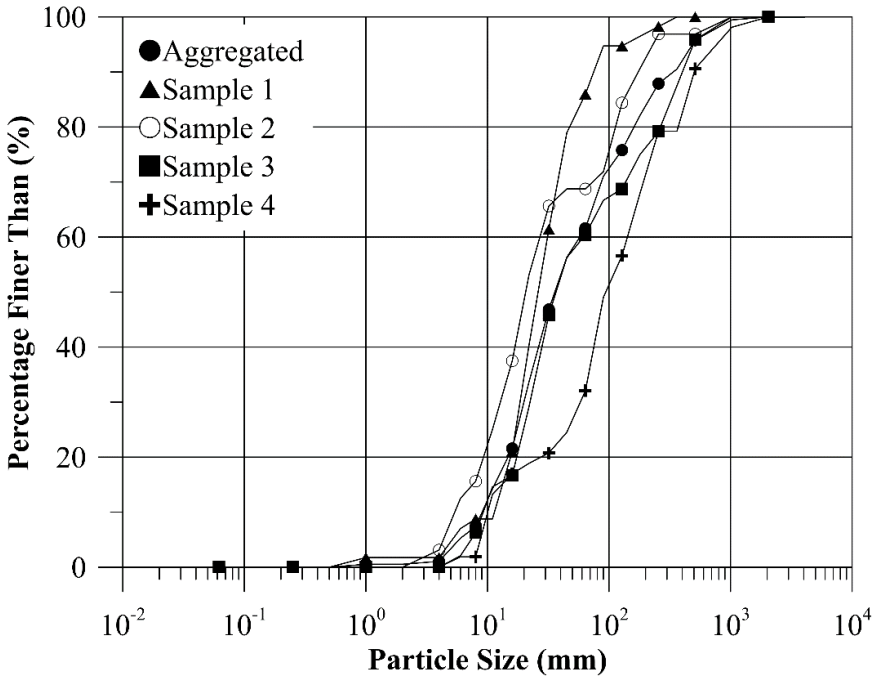

Figure 7 – Measured Grain Size distributions.

Table 3 – Grain size percentiles, roughness values and percentage of substrate type of study reach.

	Sample				
Parameter	**1 (Stn. 0+700)**	**2 (Stn. 0+580)**	**3 (Stn. 0+490)**	**4 (Stn. 0+215)**	**Aggregated**
d_5	5.10	4.34	7.13	8.73	5.78
d_{16}	13.60	8.10	11.17	14.51	11.79
d_{25}	16.95	11.00	18.76	46.00	17.21
d_{50}	25.72	20.64	32.00	94.05	34.19
d_{75}	40.63	98.28	128.00	224.32	104.23
d_{84}	53.85	126.65	213.16	418.74	176.96
d_{95}	85.22	230.33	503.20	769.35	490.29
Manning's n*	0.035	0.034	0.036	0.043	0.036
% Silt/Clay	0	0	0	0	0
% Sand	2	0	0	0	0
% Gravel	80	42	60	32	54
% Cobble	12	17	19	47	24
% Boulder	0	2	13	21	9
% Bedrock	7	40	8	0	14
Skewness (Sk_l)	-0.04	0.27	0.29	-0.09	0.21
Kurtosis (K_G)	1.32	0.74	0.91	1.16	1.01

*calculated from $n = 0.064{d_i}^{1/6}$ (Strickler, 1923)

Photogrammetry was use to supplement particle surface area measurements, owing to the highly angular and non-uniform shapes often created by plate fractures. This method corrects for variations in surface area that not accounted for in simple a·b angularity and sphericity calculations. As illustrated in

Figure 8, the sum of the surface area occupying each 5 cm grid space is less than the product of the a and b axes. The photogrammetry was completed using a raster editing and orthorectification software (AutoDesk Raster Design) and graduated makers for points of reference (AutoDesk, 2016). The depth (c plane) of each particle was based upon the manual field measurements.

The photogrammetry method predicted a 13% larger particle surface area (on average) than the product of the a and b plane dimensions. This observation relates to the propensity of limestone and shale particles to subdivide on parallel fracture planes (see Section 3.2.1). Subsequent transport relationships employing a mass component used the photogrammetric measurements of particle surface area for discrete particle volume (after integrating the c-axis).

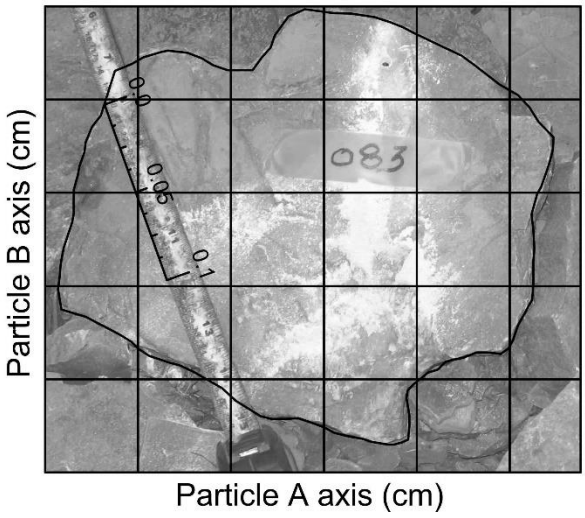

Figure 8 – Example of photogrammetric process for measurement of particle surface area. 0.05 m grid spacing.

3.3.2.1 Particle shape

Owing to the angularity of the site bed material, Sampled particles were assessed for particle shape because of its effect on critical entrainment and transport (Wilcock, 1993). Sphericity (ψ) for a given particle is defined as (Wadell, 1935):

$$\psi = \frac{s_a}{V} \tag{4}$$

where s_a (L^2) is the surface area of a sphere having the same volume as that particle and V (L^3) is the absolute volume of the particle. Wadell offers different shape variants, several of which have been appropriated for use in sediment transport studies (Julien, 1995). Julien describes a sphericity parameter for application in sediment studies, as the equivalent side of a cube having the same volume as the particle, as follows:

$$S_p = \frac{\ell_b \ell_c}{{\ell_a}^2} \tag{5}$$

where S_p= the sphericity parameter (-) and ℓ_a, ℓ_b, and ℓ_c are the particle lengths (L) for the a-, b- and c-axes, respectively. Krumbian (1941) developed a metric of particle shape by plotting ℓ_b/ℓ_a versus ℓ_c/ℓ_b. Zingg (1935) divided possible variants into quadrants, each representing different particle shape types, as per Figure 9. The particle shape data was then used in the force exceedance analysis to compare the platy particles of the study site to threshold conditions observed by others for similarly shaped particles.

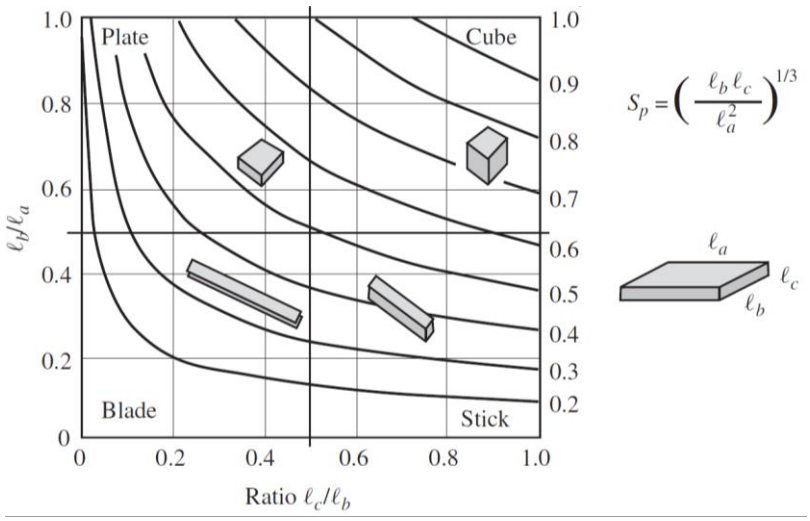

Figure 9 – Particle shape classifications, reproduced from Julien (1995).

3.3.3 Hydraulic Analysis

A one-dimensional hydraulic model HEC-RAS 4b (USACE, 2004) of the study reach was developed to assess hydraulic conditions for instantaneous peak flows that exceed the critical entrainment threshold for the smallest PIT tag seeded particle. The construct of the model assumed steady state peak flow inputs and cross sectional geometry derived from a combination of contour mapping for areas outside of the main bedrock channel, and detailed survey data for topographic definition within the bedrock channel. The model was divided into four geomorphic sub-reaches (Figure 3) to better represent the field measured bed material, specifically for reasons of roughness differentiation between sub-reaches.

Roughness values for reaches 1, 2 and 4 reach were determined from the sampled d_{50} particle size values and the Manning-Strickler formula $n \cong 0.062{d_{50}}^{1/6}$. It is noted that, for Reach 3, roughness was reduced based on a long, exposed area of bedrock in the thalweg. It is acknowledged that there are a number of other methods for estimating channel roughness (Millar, 1999), but the selected Manning-Strickler formula is representative of commonly employed engineering assumptions, speaking to the applied aspect of this study. It is also the most conservative (roughest) of the suite of Manning-Strickler expressions. Hydraulic roughness at the particle interaction level is considered by way of the shape-based threshold analysis (see Section 3.4.4) and, less directly, the particle hiding function within the sediment transport analysis.

For event-based inputs into the hydraulic model, the time series data was binned into storms then further subdivided into storms deemed to be competent (capable of entraining bedload) based on the methods described below. Because of the peakedness of the hydrology, discrete storms were easily identifiable as those exceeding the base flow of 0.10 m^3/s. For competence analysis, a storm was included if the instantaneous discharge (Q_i) (L^3T^{-1}) on the rising limb of the hydrograph exceeded the critical discharge (Q_c) for the smallest tracer particle size (d_i), and was considered to have ended when $Q_i < Q_c$. Successive rising and falling limbs did not intersect at flows greater than 0.20 m^3/s, which also coincided with the threshold discharge for the smallest tracer, based on cross sectional hydraulic model results and critical value for τ^* (derived from modified Shield diagram and equations 2 and 3) and:

$$\tau_c = (G-1)\gamma d_i \tau_c^* \quad (6)$$

Assuming a critical Shields (τ_{*c}) value of 0.054 determined from platy particle shapes ($\phi = 45$) and $d_* > 50$ (as per the Julien (2002) modified Shields diagram for determination of τ_{*c}), a critical shear stress value of approximately 25 N/m^2 was calculated for the smallest tracer particle. Using 25 L/s increments of an arbitrary peak flow, the hydraulic model was iterated at progressively larger elemental

floods, and the threshold determined to be $Q_c = 0.20$ m^3/s. This threshold discharge was found to mobilize few particles and of those identified, limited to Reach 3, but was accepted so that particle routing through higher energy sub-reach(es) were not discounted. Accordingly, the time series hydrology data was partitioned into 19 storm events (Table 4).

Table 4 – Humber Creek time series derived discrete storm event, peak flows and associated durations.

Event	Peak Discharge (m^3/s)	Start Date	End Date	Duration (hh:mm)	Particle Tacking Survey Date
	No storms observed between Aug 19 and Event 1				19-Aug
1	1.02	2011-09-01	2011-09-01	1:48	
2	8.91	2011-09-03	2011-09-03	7:48	
3	0.80	2011-09-04	2011-09-04	1:33	
4	1.31	2011-09-19	2011-09-20	10:54	
5	4.47	2011-09-21	2011-09-22	7:30	
6	8.68	2011-09-23	2011-09-23	10:21	
7	0.24	2011-09-29	2011-09-29	0:51	29-Sep
8	6.44	2011-09-30	2011-09-30	12:03	
9	6.04	2011-09-30	2011-10-01	19:24	
10	0.49	2011-10-02	2011-10-02	1:57	
11	0.25	2011-10-03	2011-10-03	1:36	
12	0.93	2011-10-03	2011-10-04	13:57	
13	4.57	2011-10-12	2011-10-14	4:00	13-Oct
14	0.53	2011-10-16	2011-10-16	2:03	
15	5.21	2011-10-19	2011-10-21	11:30	
16	0.73	2011-10-24	2011-10-24	5:21	
17	3.22	2011-10-25	2011-10-27	21:54	
18	0.22	2011-10-27	2011-10-27	1:36	
19	0.21	2011-10-28	2011-10-28	2:54	28-Oct

3.3.4 Sediment Transport Modelling

Commonly used bedload transport assumptions and formulae were applied to the shear stress exceedance and particle recovery results to elucidate the findings of this study and compare them to the results of other studies. Typically, tracer research examines the traveled distances of tagged particles and groups the results into two classes of predictive variable: 1) the physical size (or shape) of the individual clasts and 2) some model of the excess force of flow mobilizing the particle, typically expressed as peak or cumulative shear stress or stream power (Hassan and Bradley, 2015).

3.3.4.1 Size Selectivity and Particle Transport

Discrete particle tracking surveys were filtered for several parameters, including: travel distance relative to the river centreline (CL), offset from the CL, particle size, shape and mass (from sediment density and volume). Travel distances less than 1 m were culled, reflecting the sensitivity and diameter of the hoop sensor and error field of detection (MacVicar and Roy, 2011).

To correct for biases such as size skewness and event magnitude, transport distances were scaled as per the methods outlined by Church and Hassan (1992):

$$\frac{L'}{L'_{D50}} = 1.77[1 - \log_{10}\left(\frac{d_i}{d_{50}}\right)]^{1.35} \quad (7)$$

where L' is the mean travel distance (L) of the 0.5ϕ particle class i and L'_{D50} is the mean travel distance of the class that contains the d_{50} of the entire sample size. L'/L'_{D50} represents the scaled transport distance for grain sizes class d_i, normalized by the median grain size of the sample population. Wilcock (1997) noted that total displacement length is dependent on the degree of mobilization and concluded that the Church and Hassan 1992 relationship better describes partial transport conditions, and that the relation for fully unconstrained particles is likely flatter. This is because of particle hiding, imbrication and other particle interactions. MacVicar and Roy (2011) noted that fully unconstrained particles are better represented by the uniform inverse power law relationship observed by Church and Hassan (2002) of the form:

$$\frac{L'}{L'_{D50}} = \frac{\bar{d}_i}{d_{50}}^{-2.0} \quad (8)$$

The study site includes a heterogenous mix of bed form types, including zones of particle interactions interspersed with free-surface particles on bare bedrock; consequently, both Equations 7 and 8 were plotted with the scaled transport distance. This informs our interpretation of factors external to the system hydrology, including transport dependency on sediment size (Parker *et al.*, 1982), weight and shape (Komar and Li, 1986; Gomez, 1994) and sedimentary structure (Lamarre and Roy, 2008). Further, because of the stochastic nature of coarse particles transport path lengths (Einstein, 1942) and particle interactions (Einstein, 1950), results interpreted in this manner establish a basis for comparison to other studies for scenarios that are not confounded by site-specific hydraulics.

The transport distances were analyzed as a function of sedimentary structure for the first recovery period. Particle interactions are known to affect mobility by varying degrees based on the nature and significance of the interaction with significance referring to the proportion of the particle mass that is

affected by the interaction (Sear, 1996). Typical interactions at rest may include particle imbrication, clustering, or interlocking. At time of seeding, each particle was photographed and evaluated with respect to the percentage of the stone buried or otherwise constrained by a particle interaction. By this measure, the surface area of the stone was used as a surrogate for the constrained proportion of particle mass. The grain size selectivity of travel distances for three categories of particle (based on the percent of surface area exposed) were calculated, as follows:

- Constrained (> 25% affected)
- Partially constrained (between 0% and 25% affected)
- Unconstrained (0% affected)

This analysis was only applied to the first recovery event post-seeding because, otherwise, the initial resting position of the found particle was not known.

3.3.4.2 Force Exceedance and Particle Transport

τ_c^* was determined for mobile particles, assumed from particle size and shape factors as per the modified Shields diagram (Julien, 1995), and Equations 2 and 3. The peak shear stress values for relevant storm events were then derived from the hydraulic model for the observed discharges, with peak shear stress averaged across the modelled cross sections that spanned the discrete particle's travelled distance (to avoid a reach-averaging bias). In cases where a particle did not transport through multiple cross sections, the average peak shear from the nearest upstream and downstream cross sections were used. The results indicated poor agreement between the field results and the modified Shields diagram method for determining τ_c^*, including many instances where particles mobilized at $\tau^*/\tau_c^* < 1$. Because subsequent rates and volumes of transport for the site are inherently based on the modelling assumption that mobility occurs when $\tau^*/\tau_c^* < 1$, an alternative way of calculating τ_c^* was devised, using a reference shear approach.

For application of this this method, $\tau_c^* \rightarrow \tau_{ri}^*$, where τ_{ri}^* is the reference shear stress. For this study, the reference condition was determined from the applied bed shear in the recovery period having the least particle mobility. This method estimates the reference shear stress for different particle sizes based on the smallest mobilizing storm. Generally, this is a condition where particle step lengths are shorter than the overall sample. As a field-based method, this approach is analogous to other tracer studies that use in-situ bedload sampling for determining reference shear (Ashworth and Ferguson, 1989), and has the advantage of predicting different values of τ_{ri}^* for different particle sizes. This reflects the non-linearity of incipient

motion (Ashworth and Ferguson, 1989; Wilcock, 1997; Hassan *et al*., 1991). Results were averaged by 0.5ϕ grain size class for use in subsequent bedload transport estimations.

As per Sear (1996) and employing the equations and relations of Carling (1992) and Buffington *et al.* (1992), the field derived thresholds for particle classes were also compared to relationships observed by others for similarly shaped particles. Carling *et al.* (1992) used flume experiments to test critical entrainment parameters for different shaped particles. They reported pivoting angles and modes of entrainment for disc-like (platy) particles, then estimated critical shear stress based on:

$$\tau_c = \frac{2V(\rho - \rho_s)g}{\omega C_d \pi (a_2 b_2 c_2)^{2/3}} \frac{\sin(\Phi - S_b)}{cos\Phi} \frac{1}{[5.75 \log(\frac{30 z_p}{k_s})]^2} \quad (9)$$

where V= particle volume (L^3), ω is an exposure coefficient ($0.87 \leq \omega \leq 0.90$; Sear, 1992), Φ is the shape-specific pivoting angle (degrees), C_d is a drag coefficient ($1.1 \leq C_d \leq 1.2$), $a_{i=1,2,3} = \ell_i/2$ (a function of the i particle axes representing the particle surface area exposed to flow), S_b is the bed slope in (degrees), z_p is the height above the bed (L) representing the bottom of a logarithmic velocity profile and k_s is the hydraulic roughness (L). There is considerable variability in the field determination of k_s and an aggregate value of $5.9d_{50}$ proposed by Millar (1999) was employed. Empirical pivoting angle (Φ) relationships reported by Li and Komar (1986) for relative grain sizes specific to platy particles were employed in Equation 9; one each for imbricated and non-imbricated particles and the results compared to the field data.

The Buffington *et al.* (1992) results specific to friction angle for non-spherical particles were also used to test the field data against other studies. Based on empirical results from sampled bed material tested in a lab on tilting tables, Buffington reports the following equation for the threshold pivoting (friction) angle for natural substrates:

$$\Phi_n = (25 + 0.57_n)\left(\frac{d_i}{d_{50}}\right)^{-(0.16+0.0016n)} (\sigma)^{-(0.21+0.0027n)} \quad (10)$$

where Φ_n is the pivoting friction angle for the *n*th percentile and σ is the sorting parameter for the bed material, calculated as $\sigma = 3.32(\log d_{84} - \log d_{16})/4 + 3.32(\log d_{95} - \log d_5)/6.6$. Equations 9 and 10 were combined to test Buffington's observations against the field data.

For event comparisons of the field data, τ_c values were converted to τ_{*c} (based on applied shear and particle size) for each of the three platy particle scenarios above (Carling 1992-Imbricated, Carling-1992

Non-Imbricated and Buffington friction angle) and plotted alongside the field-derived τ^*_{ri} data for each grain class.

Bedload transport rates q_{bi} (kg/m/s) were normalized to the Einstein (1950) transport parameter ($q^*{}_i$) as per Ashworth and Ferguson (1989) using the method adapted from Parker *et al.* (1982):

$$q^*{}_i = \left(\frac{q_{bi}}{\rho_s}\right)\left[\frac{g{d_i}^3(\rho_s - \rho)}{\rho}\right]^{-0.5} \tag{11}$$

In this case, to integrate observed mobility for different grain classes, τ^*_{ri} was used to represent the threshold condition for grain class i, and an actual measure of particle travel distance was considered using a virtual velocity method for the rate of bedload transport (Haschenburger and Church, 1998) of the form:

$$qb_i = vD_{ac}(1-p)\rho_s \tag{12}$$

where: v is the mean virtual velocity (LT^{-1}) of a transported particle, D_{ac} (L) is the active depth of the mobile streambed and p (-) is a porosity value for the grain size mixture (commonly reported to be 0.3 for a rhombic packing arrangement (Coogan and Manus, 1975) that best approximate the bed material). For the study site, the active depth is taken to be the mean c-axis dimension for the grain class due to the lack of subsurface layer interactions (particles assumed to be traveling over bedrock). Virtual velocity, as first defined by Einstein (1937), accounts for the random nature of steps and rests experienced by saltating particles expressed by:

$$v = \frac{L_{li}}{t} \tag{13}$$

where L_{li} is the path length (L) for particles i traveled during time t, for flows assumed to be competent. The virtual velocity measure has commonly been used in sediment tracer studies as a surrogate for in-situ measurements for coarse particles that would be otherwise be difficult to trap with conventional sampling strategies (Haschenburger and Church, 1998; Ferguson and Wathen, 1998). The use of competent flow over time integrates the stochastic step nature of coarse bedload transport, a transport mode observed though the grain size dependency analysis to be dominant at the study site.

τ^*_{ri} was used to determine competence for individual particles and classes, with entraining forces based on shear-discharge rating curves developed for each of the four geomorphic sub-reaches. Equations 11, 12 and 13 were combined and q^* values and plotted against τ^*, to determine if different size fractions exhibit

similar modes of excess shear dependency. Increased separation of ${q^*}_i/d_i$ as a function of τ^* indicates that the dimensionless threshold conditions vary with grain size. The results were compared against the Wong and Parker (2006) formulation of the Meyer-Peter and Müller (MPM) dimensionless bedload transport formula:

$$q^* = 4.93(\tau_* - \tau_{*C})^{1.6} \tag{14}$$

where q^* (-) is the dimensionless sediment transport rate per unit bottom width (the Einstein normalizing parameter) and τ_* and τ_{*C} are dimensionless shear stress and critical dimensionless shear stress, respectively. For reasons of empirical derivation, the M-PM formula is considered applicable for coarse grain sediment mixtures having low or no sand content (Willcock *et al.*, 2009), conditions found at the study site. Other transport models were considered (Parker *et al*., 1982; Wilcock and Crowe, 2003) but ultimately discounted due to the absence of contiguous bed roughness along the channel bed or due to the lack of sand size fraction in the bed material load respectively.

The Egiazaroff (1965) hiding factor was applied to account for particle interactions, as per Ashida and Michui's (1972) observation that smaller relative grain sizes are more difficult to mobilize, generally at $\frac{D_i}{D_{50}} \leq 0.4$, and was formulated in the following form:

$$F_h \begin{cases} 0.843\left(\dfrac{d_i}{d_{50}}\right)^{-1} \; for \;\; \dfrac{d_i}{d_{50}} \leq 0.4 \\ \left[\dfrac{\log(19)}{\log\left(19\dfrac{d_i}{d_{50}}\right)}\right]^2 \; for \;\; \dfrac{d_i}{d_{50}} > 0.4 \end{cases} \tag{15}$$

where F_h is the hiding function applied as a factor of the d_{50} grain size for determination of class-based τ_{*C} values, which are then used in the subsequent estimation of q^*. The hiding function is a commonly employed method that considers particle interactions using an expression of relative roughness in relation to the median bed material size. The hiding function is then used to normalize the critical shear values for each grain class based on the D_{50} threshold. In this case, the field calibrated d_{50} threshold was used.

Dimensionless bedload flux was also weighted for bed abundance of different grain size fractions as per the Einstein (1950) dimensionless form and fractioning methods adapted from Parker *et al.* (1982), as per:

$$q_i^* = \frac{qb_i}{f_i\sqrt{(G-1)gd_i}d_i} \tag{16}$$

where qb_i ($L^2 T^{-1}$) is the transport rate and f_i (-) is the fraction of bed material (based on the grain size distribution for mobile particles in this case) corresponding the i^{th} grain size class and d_i (L) is the mean size of the particle class. Solving equation 16 for qb_i allows for calculation of the weighted bedload transport rate:

$$qb_i = q_i^* f_i\sqrt{(G-1)gd_i}d_i \tag{17}$$

Transport rates were plotted as a function grain size to compare the field results, which inherently account for size selectivity, to the empirical hiding function model. The virtual-velocity based model was also includes in this comparison.

3.4 Results

3.4.1 Tracer Recovery

The tracer results yielded excellent total recovery rates (N_t) for the first two tracks post-seeding (89% and 91%, respectively), which then diminished to approximately 70% for tracking periods 3-6 (Table 5). Tracking period 3 occurred after spring a freshet and the drop-in subsequent recovery rates may be associated with particle transport and sorting during this event that moved beyond the study limits. P_m was considerably less than the total percent recovered, with the highest percentage found during Event 3 (68%). The mean transport distance for all mobile particles was also highest for Event 3, averaging 76 m. The fewest number of mobile particles were found in Event 6, which included only one paired particle. Consequently, Event 6 was omitted from future event-based analysis.

The D_{50} size of mobile particles was generally consistent, with the average transported particle for all the events being large cobble (-7.5ϕ to -8.0 ϕ), except for Event 6.

Table 5 – PIT tag summary: recovery and mobility results.

Recovery Event	Date	N_t	P_t (%)	N_{EVB}	N_m	P_m (%)	L_{mean} (m)	L_{d50} (m)	d_{mobile} (m)
0	2010-07-22	250	-	-		-	-	-	
1	2010-10-02	222	89	220	49	22	33	28.4	209
2	2011-02-17	228	91	209	14	12	8	1.7	272
3	2011-08-19	178	71	166	111	68	76	94.3	274
4	2011-09-29	186	74	157	20	21	43	76.8	297
5	2011-10-13	184	74	167	7	7	7	2.2	196
6	2011-10-28	186	74	163	1	4	327	n/a	85

250 total seeded particles in Recovery Event 0; N_t is the total number of found particles; P_t is the total percentage of found particles; N_{EVB} is the number of particles also found in the preceding recovery event; N_m is the number of mobile particles (based on N_{EVB} cases only); P_m is the percent of particles found to be mobile; L_{mean} is the mean path length for each period; L_{d50} is the mean path length of the particles containing the d_{50} grain size class; and d_{mobile} is the mean mobile particle size for each recovery event.

A thorough review of each particle transport case was undertaken to identify anomalies that may misrepresent the overall transport relationship, including an assessment of total particle distance travelled, stone size and type, and photos of the stone positioning during seeding. Identified anomalies included instances where the glass PIT tag capsule dislodged from the tagged particle, or where larger clasts have fractured into smaller pieces. Both occurrences anomalously report longer-than-true distances and, as a result, seven particles were removed from the data set for the following reasons:

- 5 medium boulder (-9.0 to 9.5 ϕ) particles were removed where$10 \leq L'_{D50} \leq 60$. It is assumed that particle desiccation or PIT tag dislodgement occurred in these instances.
- 2 particles were omitted from the transport analysis because they were installed in the headcut face (within the intact bedrock) to look for capstone cavitation or undermining.

The total recovery results compare favourably with those observed by other recovery studies (Hassan *et al.*, 1991; Lamarre *et al.*, 2005; Bradley and Tucker, 2012; Schneider *et al.*, 2014) using passive recovery strategies (either magnetic or PIT tag technology). The percent mobility results for Events 1 – 4 were also within the range of other studies, while Events 5 and 6 generally had lower comparable mobility.

The grain size distribution for mobile and immobile tracer particles and overall bed material distribution are plotted in Figure 10. As previously noted, this distribution and the percentile sizes (Table 6) are not based on a randomized sample set and the results support the tracer experiment only. There is a slight fining of nearly all particle size fractions for the mobile particles, as compared to the total group of seeded particles, although the distributions are very similar. This indicates that the population distribution of seeded particles generally agrees with that of the subset of seeded particles determined to be mobile. Unknown is the sample distribution of mobile particles finer that the smallest seeded particle for reasons identified by Houbrechts (2012).

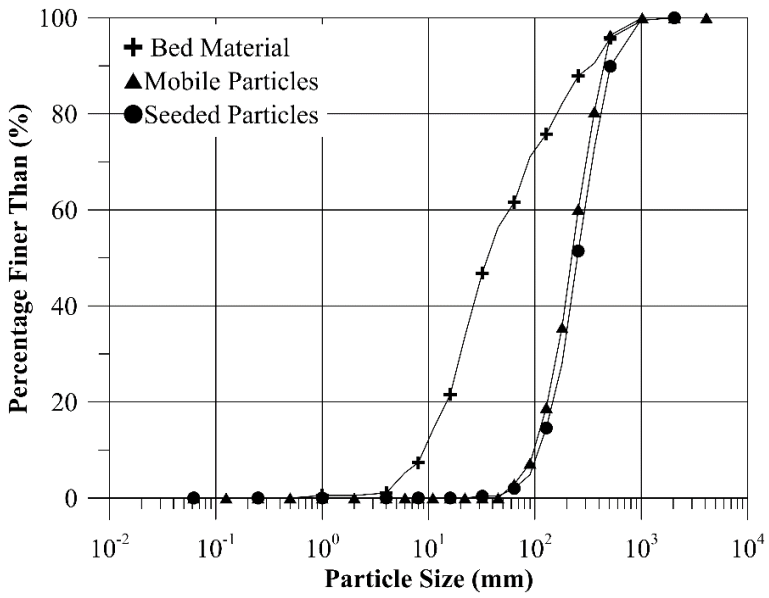

Figure 10 – Cumulative grain size distribution for the native bed material, particles seeded for PIT tag tracking, and mobile-recovered particles

Table 6 - Percentile particle diameters for particles seeded for PIT tag tracking

Percentile Diameter	Seeded Particles (mm)	Mobile Particles (mm)
d_5	90.46	77.86
d_{16}	132.74	123.18
d_{25}	167.01	153.35
d_{50}	250.62	233.92
d_{75}	378.03	353.79
d_{84}	454.17	430.29
d_{95}	727.09	673.92

3.4.2 Particle Shape

Figure 11 illustrates the general shape classification of the sampled particles, confirming a clear bias towards the disc or "plate" quadrant. Using equal quadrant divisions to tally individual particle shape classifications, 68% of the 436 sampled particles have a plate-like shape, supporting the contention that the subsequent hydraulic and sediment transport analysis of study reach is atypical with respect to the body of scientific research in this field. Particle shape data was used to compare the study site transport characteristics against other observed relationship specific to disc or plate-like particle shapes (see Section 3.3.4.2).

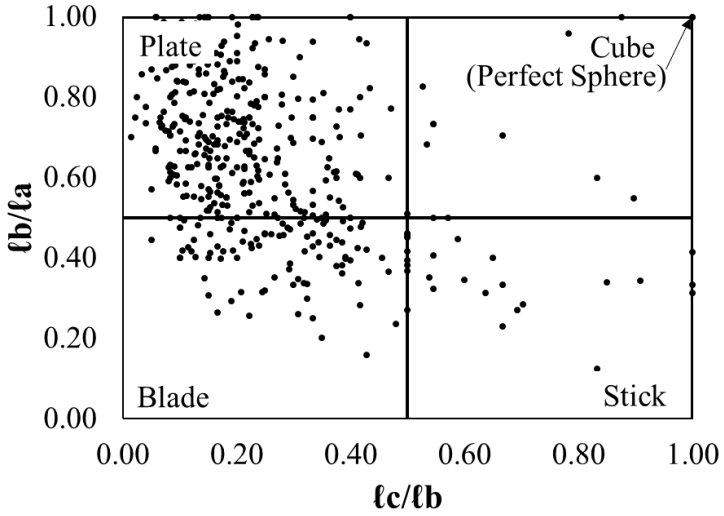

Figure 11 - Particle shape factor classifications based on particle axis length ratios (Julien, 1995). Quadrant divisions shown.

The results of the PIT tag experiment were divided into two observational sets: 1) tracer movement as a function of particle size and 2) tracer movements as a function of applied shear stress for storm events exceeding a reference critical shear stress (see section 3.4.4, below).

3.4.3 Size Selectivity – Transport Dependency

Class-based seeding and transport distance results were log-transformed to obtain results that are less statistically biased by extreme observations (MacVicar and Roy, 2011) and were all confirmed to be normally distributed (Kolmogorov–Smirnov test; α=0.05).

Table 7 identifies a trend of decreased path lengths corresponding to increases in particle size. The D_{50} size for all seeded particles forms part of the 'very large cobble' fraction, a class in which 71% of the particles were mobilized, having a mean travel distance of 63 m. This class also included the most seeded particles (58). The percent mobility decline is generally consistent for the grain size classes between -6.0ϕ and -9.0ϕ, with a sharp drop decline at the medium boulder (< -9.0ϕ) class.

Table 7 – Summary of particle mobility by 0.5ϕ grain size class for all tracking periods.

Size Class Description	ϕ	NC_m	PC_m (%)	LC_{mean} (m)	PC_{mean} (mm)
Small cobble	-6.0 to -6.5	7	71	95	80
Medium cobble	-6.5 to -7.0	24	79	86	108
Large cobble	-7.0 to -7.5	33	76	64	154
Very large cobble	-7.5 to -8.0	58	71	63	208
Small boulder	-8.0 to -8.5	53	64	59	307
Small boulder	-8.5 to -9.0	42	62	29	410
Medium boulder	-9.0 to -9.5	25	36	41	662

NC_m is the total number of seeded particles for each class; PC_m is the percentage of particles in a class found to have mobilized at least once; LC_{mean} is the mean path length for each class (based on N_{EVB} cases only); and $PC_{mean}$is the mean particle size for each class. Class descriptions are as per the Wentworth Scale.

When compared to the overall grain size distribution of seeded particles, the cumulative mobile fractions agree with respect to the grain size distribution (Figure 10). At the 50th percentile, only a 10% reduction in grain size from the seeded distribution to the mobile distribution was observed, a disparity that is generally consistent between sizes bounding the second moment of variance (ϕ_{84} and ϕ_{16}). Compared to the bulk bed material, there is a clear difference between the native bed material and the

seeded / mobile particles, with the tracer data being biased towards the coarser grain sizes. Notwithstanding this disagreement, it is worth restating that the seeding process attempted to visually match the natural distribution of bed material; however, the technical constraints of the seeding process inherently biases the results towards coarser particles (due to the difficulty of PIT tag insertion in smaller stones). In particular, the geologic origin of most smaller particles is fractious shale, making PIT tag seeding impossible.

To illustrate the distribution of transport distances for different recovery events, discrete event-paired (N_{EVB}) particles were binned into 5 m long transport distances and their relative frequencies plotted (Figure 12). These distributions do not include particles that remained immobile. The relative frequency of mobile particles is clearly dominated by recovery Events 1 and 3, with the number of particles found to be mobile decreasing significantly in Events 2, 4 and 5. The Events, however, do provide an indication of the distances associated with the lower spectrum of threshold mobility. Most particles moved distances less than the overall mean ($L'_{D50} = 57$), with less frequent occurrences of much longer travel distances observed.

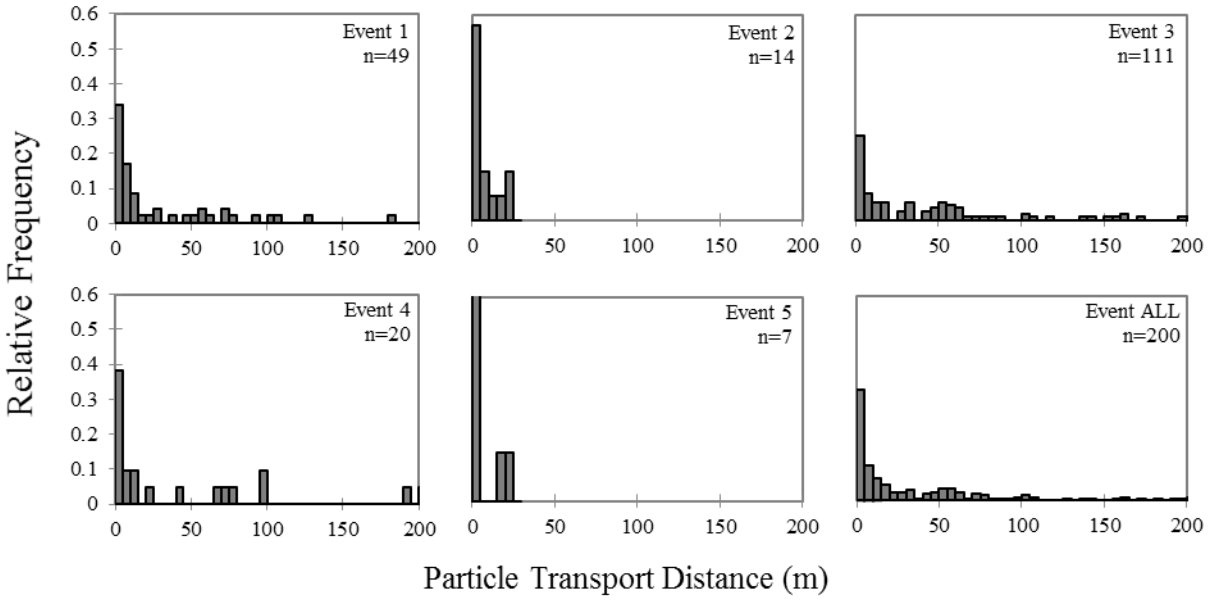

Figure 12 – Particle transport distances per recovery event for mobile particles (N_{EVB}). Lengths binned into 5 m travel distances. Number of found particles shown.

Figure 13 shows the cumulative travel distances for all recovery events (mobile particles only), with data binned into 25 m increments to illustrate frequency distribution of the mobile particles. A variety of

bin sizes were explored to test different models of frequency distribution for added insight into explanatory variables, but no added value was perceived from smaller or larger bins.

The 25 m bin clearly dominates the distribution, with a third of the population occupying the smallest of particle size bins. The distribution also shows slight clustering around the 100 m and 275 m lengths. Observed travel distances were fitted with a two-parameter gamma distribution for visualization and owing to this distribution commonly representing stepped travel distances in similar studies (Hassan *et al.*, 1991, Liebault et. al., 2011). Goodness of fit was tested (p = 0.049) using the Kolmogorov-Smirnov (K-S) and chi-squared methods at a significance level of α=0.05, resulting in the gamma distribution not being rejected by K-S and approximately meeting the *p* value criteria for chi-squared (p=0.049). Here, a shape parameter k=0.6 representing the dominance of the shorter path lengths was found to best represent the distribution. The cumulative plot shows an inflection approximately at the 80th percentile (corresponding to the 125 mm particle size) above which there is a tailing off of the relative contribution of longer travel distances.

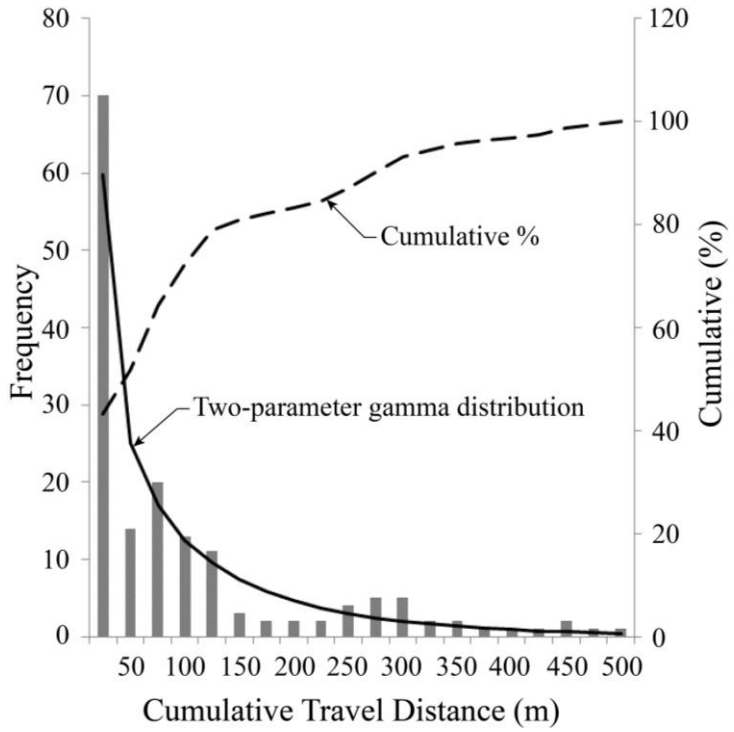

Figure 13 – Absolute and cumulative frequency of travel distances for all events. Two-parameter gamma distribution shown as solid black line.

Discrete particles were then aggregated based on the Wentworth system for analysis by 0.5ϕ size classes. Figure 14 illustrates the transport dependency for the 7 size classes identified in Table 7 for particle diameters ranging between -6.0ϕ (64 mm) and -9.5 ϕ (724 mm). These data were log-transformed and the null hypothesis for normal distribution (K-S test) of discrete recovery events was not rejected. Linear correlation between both dependent variables (transport distance and percent mobility) and grain size class was found to be significant ($p < 0.05$). The variability for transport distance is less attributable to size class than is the case for percent mobility (R^2 was 0.68 and 0.83, respectively). The results also indicate a steepening of the path length trend at the approximate -8.0 ϕ grain size class, a case also observed in the scaled relationships reported later.

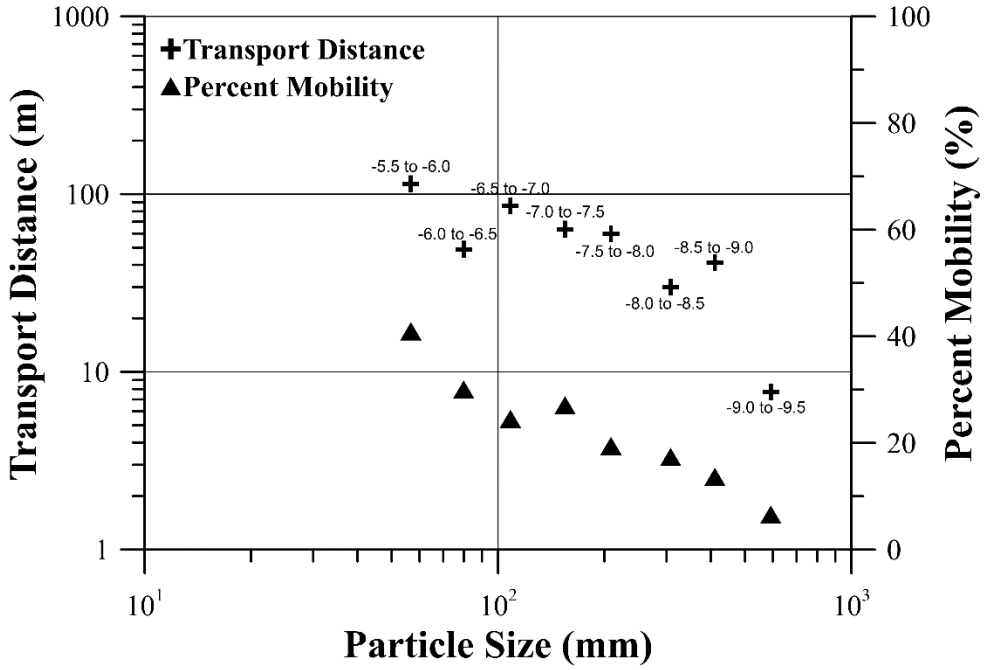

Figure 14 – Transport distances and percent mobility for 0.5ϕ grain size classes. 0.5ϕ grain size classes are labelled.

Figure 15 shows the grain size selectivity of travel distances for three categories of particles, based on the percent of surface area constrained, partially constrained or unconstrained. The correlation for unconstrained particles was tested to be significant at α=0.05, but this was not the case for either of constrained cases. Figure 16 illustrates the effect of grain size selectivity on scaled transport distances, using scaling methods employed by Church and Hassan (1992). The data was tested to be normally distributed before comparing to relationships developed by others. Because the study site includes a heterogenous mix of bed form types, including regions of particle interactions interspersed with free-

surface particles on bare bedrock, both equations 7 and 8 were plotted for comparison with the scaled transport distances (Figure 16). The standard error bars reflect the dispersive nature inherent to particle tracking, but the data show a discernable trend that plots below the Church and Hassan partial mobility function. However, there is disparity in the scaled transport relationships for fine and coarse particles, differentiated in this case by the fifth largest particle class (very large cobble having a mobile D_{50} of 208 mm). This decline is also evident in the Church and Hassan 1992 relationship (as per equation 7), however, Figure 16 indicates the study site has a steeper trend than the inverse squared reported in the literature, a condition also supported by the unscaled transport distances plotted in Figure 14.

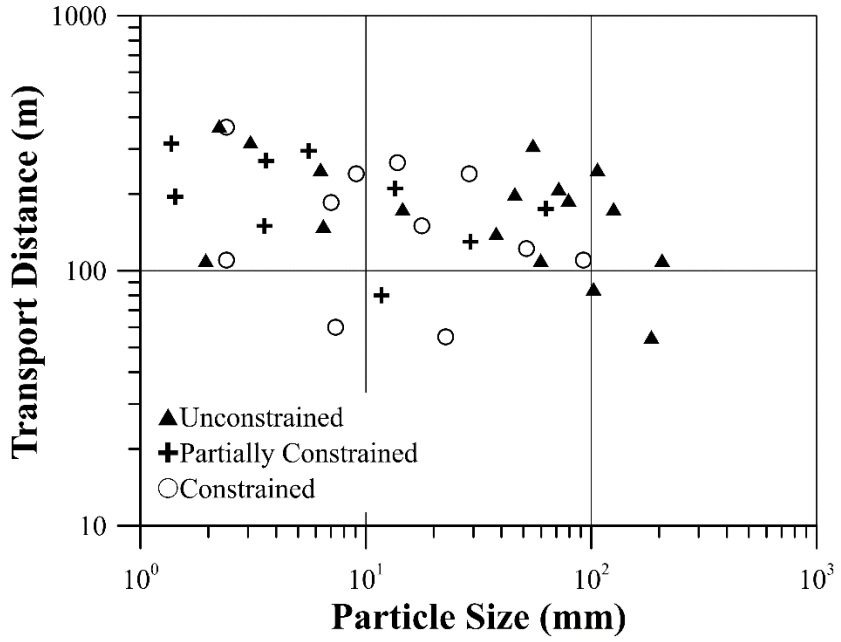

Figure 15 – Transport distance for constrained, partially constrained and unconstrained particles, as a function of grain size

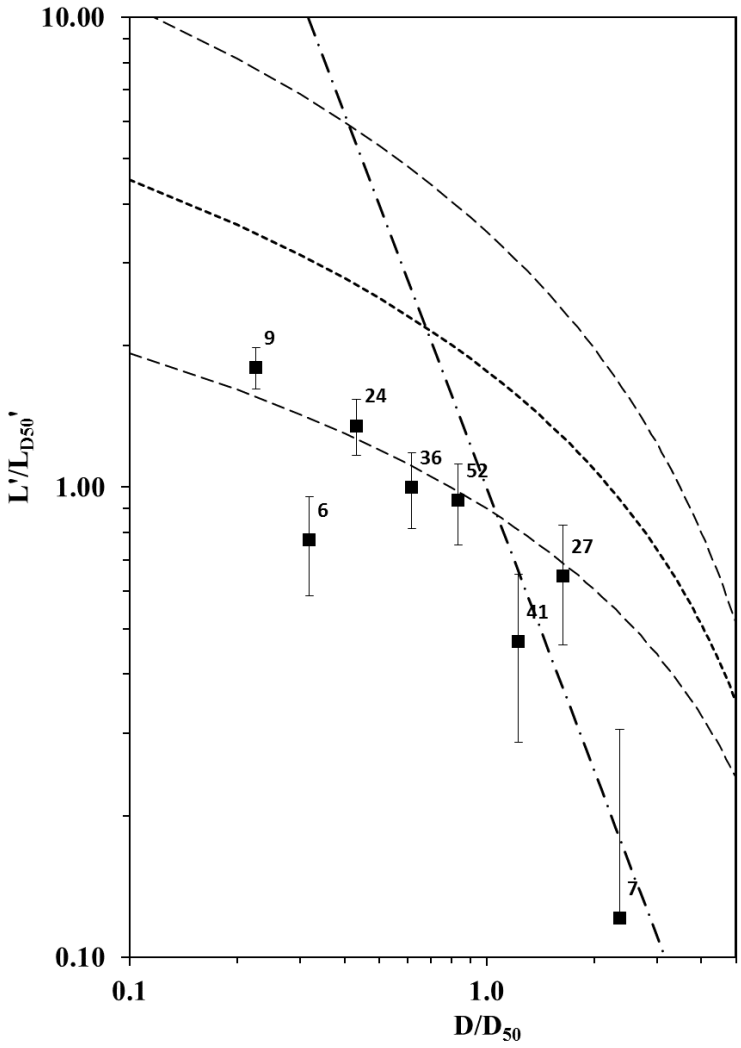

Figure 16 – Scaled transport distances for 0.5ϕ grain size classes (all events). Standard error indicated. Partial mobility results of Church and Hassan (1992) are shown with confidence intervals α=0.05. Equation 8 (for unconstrained clasts) is also shown as a straight line.

3.4.4 Force Exceedance – Transport Dependency

Empirical-based critical shear values (τ_c^*) reported in the literature for coarse gravel particles did not agree with the observed mobility results. Figure 17 illustrates this case, where most mobile particles fall below the assumed threshold for mobility, indicating the value of $\tau_c^* = 0.054$ derived from d_* over-predicts incipient motion for most parties in the study site, precipitating the need for further investigation into the critical shear values for the study site.

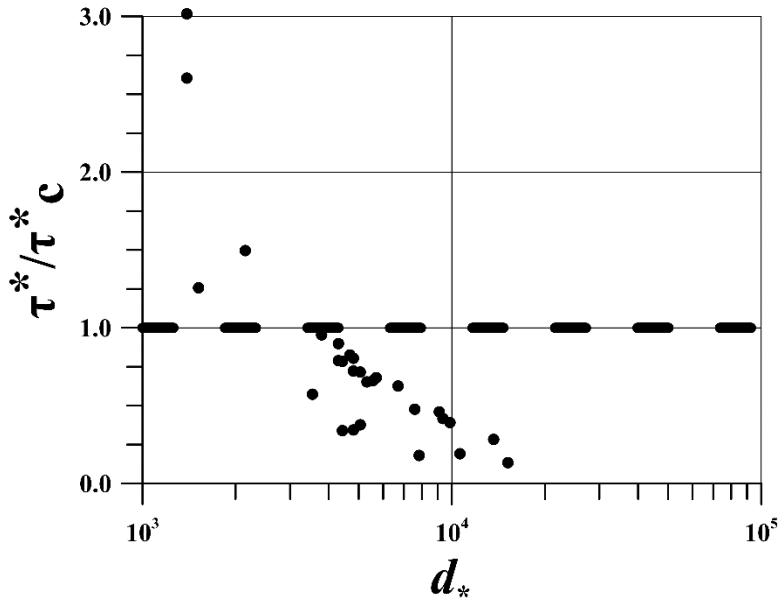

Figure 17 - Critical shear stress exceedance ratios for mobile particles (N_{EVB} cases only), as function of particle size. τ_c^* assumed as per modified shields diagram (Julien, 2002). Threshold of mobility $\tau^*/(\tau_c^*) = 1$ plotted as a thick dashed line for visualization.

Figure 17 demonstrates the case for an alternative means of calculating τ_c^*, in this case using a reference shear approach to predict τ_{ri}^*. The results of this analysis are plotted in Figure 18, along with the originally predicted value for $\tau_c^* = 0.054$ (dashed line) based on the modified Shields diagram (Julien, 2002). The plots shows a decreasing dependency on grain size (or potentially ρ_s as the other variable in the τ^* denominator) for critical values of τ^*, as grain size class size increases. These findings support the grain size selectivity results plotted in Figure 16, with potential reasons addressed in the discussion regarding the increased differentiation (from the gravel-based models reported in the literature) by size class, as coarseness increases at the study site.

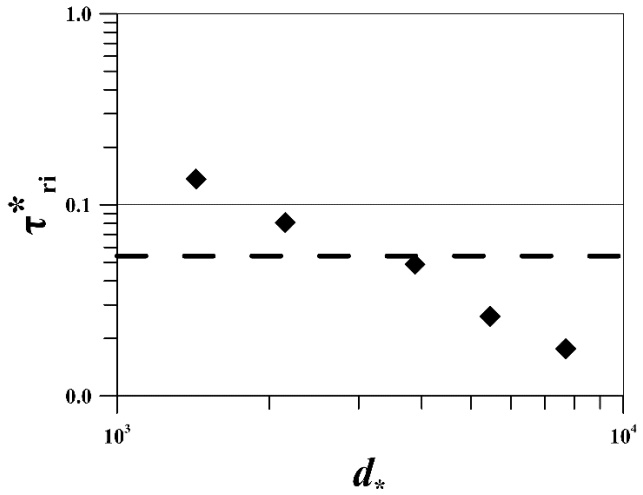

Figure 18 –Reference shear stress values for 0.5ϕ grain classes, as a function of grain size. Modified Shields threshold condition (Julien, 2002) plotted as dashed line for comparison.

With respect to incipient motion, the field-calibrated results were then compared to transport relationships observed by others for similarly shaped particles. Figure 19 indicates that the class-based field results agree well with the empirical relationship for platy, imbricated particles determined by Carling in flume studies. Comparatively, Carling's observations of unconstrained platy particles predict a lower incipient threshold for all classes. Likewise, the Buffington model for platy particles having sphericity values calibrated to the study site predict even lower thresholds.

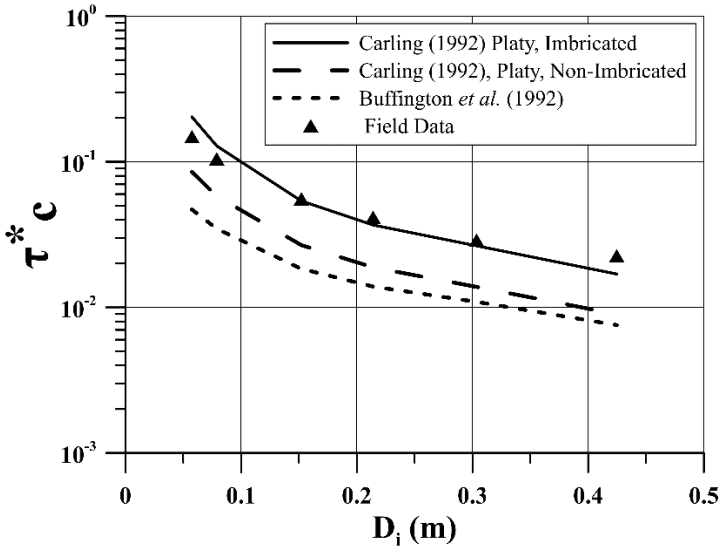

Figure 19 – Field calibrated critical Shields values compared against empirical relationships. Carling (1982) is specific to platy particles. Buffington data is based on non-spherous particles and related pivoting (friction) angles.

Using the reference shear values determined form the field data, dimensionless bedload was calculated as a function of τ_* (Figure 20). Separation is visible between the different grain classes, which is indicative of the degree of size selectivity. The Parker-Wong corrected M-PM equation is also shown as a point of comparison, including a single grain class (-8.5ϕ to -9.0ϕ) using the field derived reference threshold, as well as a continuum of M-PM predicted transport values for the modified shields diagram threshold of $\tau_{*c} = 0.054$ (that corresponds to the site's grain size). This class was used as an example, and indicates that the data points plots to the left of the relationship using M-PM (i.e. smaller shear values generate the same predicted bedload transport).

Disparity is evident between the two dashed lines, indicating that the field results depart not only from the size selectivity relationships observed by others (Figure 16), but also from a commonly applied (M-PM) bedload transport relationship for both literature-derived shear thresholds and for M-PM using site-specific particle sizes. The plotted τ_{*ri} M-PM continuum has been shown only for one grain size class, but it is evident that the coarsest grain sizes (>-6.5ϕ) all left of the M-PM relation that uses the common methods.

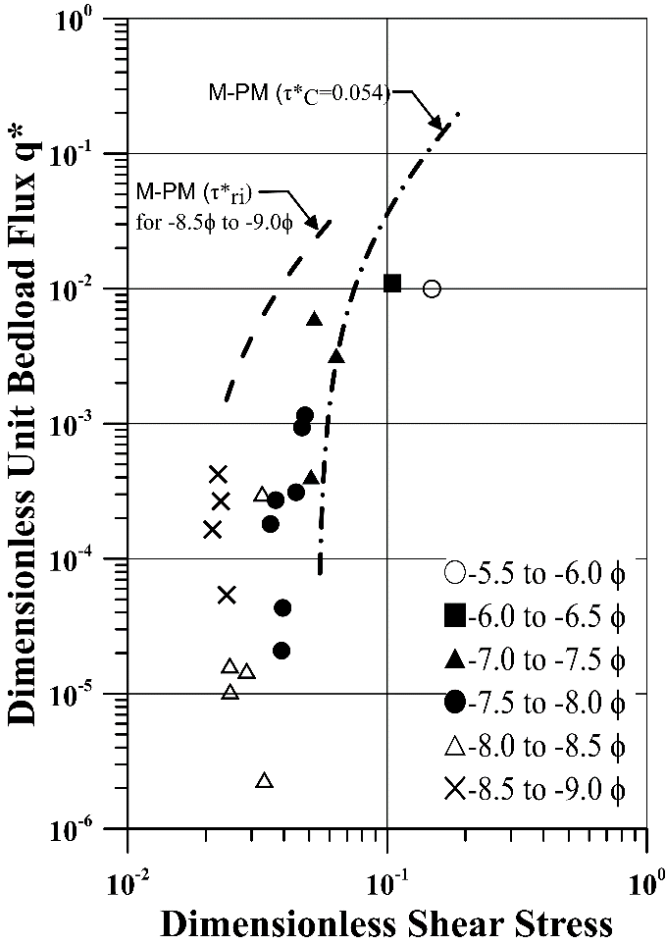

Figure 20 – Dimensionless bedload flux dependency on τ_* by 0.5ϕ grain class. Single grain class (-8.5 to -9.0ϕ) using Parker-Wong corrected M-PM relation is plotted to illustrate relation (dashed line). M-PM continuum assuming $\tau_{*c} = 0.054$ is also plotted for visual comparison (dash-dot).

The results were then analyzed in the dimensional form for 0.5ϕ grain class transport rates. Three methods of expressing transport rates using field data are plotted in Figure 21.

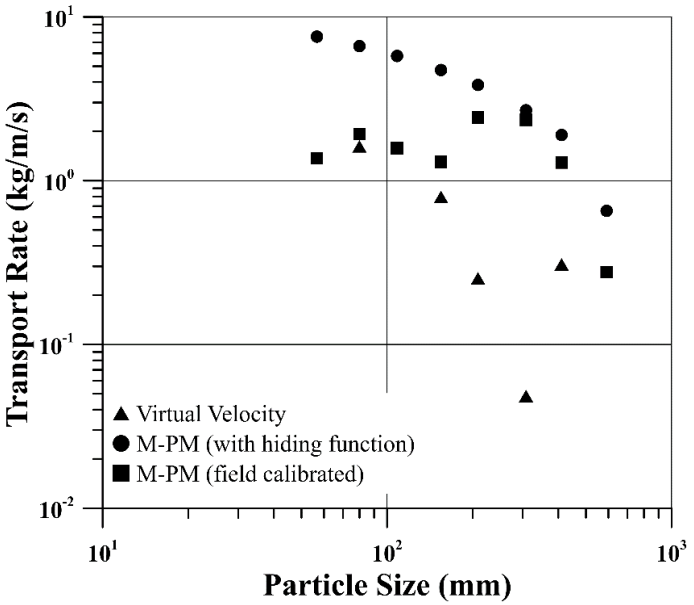

Figure 21 – Bedload transport rates as a function of grain size. Rates as determined by three methods: virtual velocity, M-PM (using a hiding function referencing the observed D_{50} τ_{*c}) and M-PM using field calibrated reference shear values).

It is interesting to note that the field derived D_{50} value for τ_{*c} corresponds to the original normalizing parameter suggested by Ashida and Michiue (1972) of 0.05 (field data indicated 0.049). The transport rates indicate agreement between the field calibrated transport rates and those integrating the hiding function, for particles larger than 200 mm diameter. For smaller particles, there is a clear departure in the relationship, where particles smaller than 200 mm transport at rates 2-3 times less than is predicted by the M-PM relationship. The M-PM rates decline with particles size at a steadier rate than do the field-observed rates, which is indicative of the normalizing effect introduced by the particle hiding function. These results suggest that the particle interactions at the study site are more effective at decreasing transport rates for smaller particles, than is the case for methods commonly cited in the literature.

The virtual velocity based rates are plotted as points of comparison. They show more scatter among the grain classes than do the field calibrates, but also a general trend of decreasing rate for larger particles. Potential reasons for the increased scatter are provided in the discussion.

In summary, the results indicate that the initiation of movement and transport of particles in the study differ from empirical results reported by others, which have been typically developed in gravel-bed systems or laboratory flumes. The comparison indicates that size selectivity and force exceedance models predict larger particle are more readily entrained (by a factor of approximately 2.6) and move shorter step lengths than would otherwise be predicted by the literature.

Chapter 4
Discussion and Conclusions

Several methods were employed to assess the bed material transport dynamics of coarse particles in a bedrock channel, which were identified to have entrainment thresholds and size selective transport dynamics that differ from many published empirical relationships. Field derived, threshold conditions for coarse particles (> the D_{50} class) diminished by a factor of approximately 2.6, when compared to the modified Shields relationship for particle entrainment. The inverse was true for finer particles. Common models for estimating sediment entrainment and transport have typically been derived from gravel-bed systems or from laboratory settings approximating gravel-bed dynamics which notably differ from the study site. Because these relationships are used to solve sediment transport problems, the experimental findings have implications for engineering applications within these types of hydrological and lithological settings.

The current field study identifies that the grain size distribution of transported particles approximated the seeded population, but was coarser than the overall distribution of bed material. This suggests that the selection of tracer particles was effective in mimicking particles likely to transport, but only for coarser fractions (owing to the inherent limitations of PIT tag seeding technology). This finding was, however, in keeping with the study objectives of principally examining the coarse particle transport dynamics thus the bias is acknowledged and accepted.

The frequency of particle travel distances conforms to a two-parameter gamma distribution (a common method for dividing and analyzing transport data), suggesting that the stochastic step lengths themselves have frequencies that are distributed in a mode agreeing with other tracer studies. With respect to grain size selectivity, a two-phase relationship between grain size and transport distance was observed in two analyses, first by the relative shorter transport distances of coarse particle classes within the field data (Figure 14), and then in the scaled relationships when compared to other studies (Figure 16). These two modes are differentiated by finer particles that behave similarly to constrained clast relationships observed by Church and Hassan (1992) (Equation 7), and coarser grain transport distances that are more indicative of unconstrained conditions. While Church and Hassan (1992) and others (Ferguson and Wathen, 1998) differentiate between scaled travel distances and grain size dependency at or around the median grain size (whereby the steepness of the function diminishes with particle coarsening), the study site indicates a more pronounced relationship than the literature typically suggests. The results also agree with general findings of non-linearity of transport rates between particle classes, and non-conformance

with flume derived critical shear values for heterogeneous, coarse sediment mixtures (Church and Hassan, 2002). Particle interactions are likely factors in the constrained versus unconstrained inter-class parity, and a test of the particles identified as initially constrained (imbricated, buried, etc.) found statistical significance for unconstrained travel lengths, but rejection of the null hypothesis for constrained particles and their respective steps lengths. It is acknowledged that this test was limited to initial mobility only, as subsequent surveys did not identify a particle as being either buried or not, but the results were notable and support the conclusion of transport differentiation.

Force exceedance results were then tested against the grain size specific findings, and it was noted that as d_* increases the data trends away from the anticipated threshold of mobility at $\tau^*/(\tau_c^*) = 1$. Indeed, there were many cases where particles transported under assumed immobile conditions ($\tau^*/(\tau_c^*) < 1$, when using the modified Shields relationship (Julien, 1995). Thus, an alternative method to better reflect particle mobility from the field data and bedrock channel morphology was employed. A reference condition was identified for several grain size classes, allowing for field calibration of the force exceedance analysis. This also allowed for computation of particle rates using the virtual velocity method which, because of its integration of multiple, stochastic, steps, is believed to be a preferred way to represent the disparate and heterogenous constrained versus unconstrained site conditions.

The field calibrated thresholds were compared to the findings of others based on particle shape which showed excellent agreement with empirical findings of Li and Komar (1986) for imbricated platy particles. Carling's (1992) observations of platy particles, being the most likely (of the shape classifications) to imbricate, also agree with the conditions observed in the study site. This agreement further supports the use of the reference-based method for estimating size selective thresholds. These comparisons suggest that the particle entrainment conforms to observations for same-shape particles in laboratory settings, an interesting finding because it narrows a gap in the scientific literature with respect to field-based particle shape data.

A comparison of the dimensionless transport rates to shear stress (Figure 20) using methods employed by Ashworth and Fergusson (1989) further supports the case of increased coarse particle transport, in this case where same transport rates are predicted for small and large particles alike. In this case, the M-PM model was used as a basis for comparison. The plot reveals clear separation between each grain class (and indication of grain size selectivity), but the classes are not stacked vertically, again indicating a bias towards coarse particle transport. This is likely a result of particle hiding reducing fine particle transport and the diminishing τ_{*c} relationship with increasing grain size, an effect that was further revealed through the bedload flux analysis (discussed below).

Dimensionless grain size analysis was also evaluated in terms of virtual velocity-based rates for comparison. As a common method for analyzing tracer data, the objective was to ascertain if the field data agrees with other researchers' findings. It does not. The overall shape of the relationship conforms with the field data, but the increased scatter suggests that, although this method is commonly applied in gravel-bed tracer studies, it may be less applicable to the study site. This may be due to the wider spread of critical entrainment thresholds between grain classes or to the more erratic nature of step distances. The presence of frontrunner particles having been transported long distances may also be biasing the virtual velocity based results. There were some front runner particles in each of the particle classes.

Figure 23 compared rates determined from field calibrated shear thresholds to those implicitly incorporating a hiding function. Based on the agreement with imbricated threshold conditions and the finding of short step lengths but increased coarse particle transport, the results here support the conclusion that particle interactions are a major factor affecting sediment transport rates. This observation further confirms an increased hiding effect for smaller clasts within the field data, as compared to results of other studies. For larger particles, the results indicate that particles transport at rates that can be predicted by commonly applied shear exceedance models (those considering particle hiding). This contrasts with the smaller particles, which consistently transport at lower rates than would be predicted. These results suggest increased efficacy of particle interactions in reducing transport as particle size decreases, when compared to common analytical methods. These interactions may be the result of any number of bed form arrangements that were observed.

One explanation for the observed effectiveness of particle interactions on transport rates is the complex bed morphology characterized by frequent and intermittent bed structures that have coarse keystone-like features which maintain local grade control. Sedimentary structures such as these were observed by Wathen *et al.* (1997) to be rapidly organizing features, and Lamarre and Roy (2008) noted the significance of clasts clustering around larger particles, acting as keystones (a condition also observed in the study site). The increased propensity for the platy particles to imbricate, combined with the relatively low critical shear once unconstrained, may be affecting the step-rest sequences in ways that differ from coarse gravel-bed systems. Particle shape also has the effect of increasing interlocking by blocky particles, meaning that the entrainment of smaller grains, once hidden, is less probable than for larger grains of a similar relative grain size.

Coarse sediment transport occurs in a series of steps and rests by discrete particles, subject to a probabilistic relationship between applied and resisting forces (Einstein, 1937). The probability of particle entrainment and exchange between geomorphic units is confounded by particle interactions. At the study

site, the results suggest that these interactions have a greater effect on small particles (a relationship observed by others), but coarse particles are also observed to transport shorter relative distances than the literature would predict. One possible explanation for this is the mode and frequency of particle exchange between heterogenous bed forms. The bed forms tend to have non-uniform shape and periodicity, that is predicted to interrupt the series of steps and rests This effect is analogous to investigations into discrete forcing features in step-pool systems using tracers (Lamarre and Roy, 2008, Lamarre *et al.*, 2005), where the longitudinal complexity of step-pools suggests randomness of transport though these units, and overall shorter step lengths than is reported for riffle-pool systems.

At the study site, the bed form complexes are not only irregular and non-uniform, but include segments of exposed, bare bedrock providing fully unconstrained environments for particles to mobilize as per the relationship seen in Figure 16. These bare patches provide completely unconstrained raceways for particles due to the diminished roughness. The net effect is alternating sequences of high and low constraint. The unconstrained instances of particle transport predicts increased mobility for these sub-reaches, but the scaled results indicate decreased size selective transport for coarse particle. Thus, the complex bed forms must be resulting in prolonged rest periods in these units, when compared to gravel-bed studies reported in the literature. This intra-unit rate of particle exchange would benefit from more study specific to bedrock systems.

The effects of reach-scale bed form heterogeneity is also known to influence sediment transport (Goode and Wohl, 2010). Bedrock controlled, abrupt changes in morphology (both in plan and profile) are common in the study site, and may govern local instances of flow acceleration that could confound the overall transport results. Further, the episodic nature of bedrock degradation for interbedded systems will result in abrupt changes that may catalyze rapid transport over short periods of time, followed by long rest periods. Cavitation of capstone, while exposing softer sediment to entraining forces, is one factor that could be contributing in this respect. Further study into the antecedent mechanisms govern these episodes would narrow the research gap in this respect.

The implications of these findings for applied sediment transport problems are varied. Sediment entrainment and transport dynamics are directly linked to channel form development (Leopold and Maddock, 1953), and we can deduce that commonly applied hydraulic geometry relationships employed in river rehabilitation projects will not predict a stable discharge regime for sites having similar hydrology and lithology as the study site. The natural tendency for platy particles to imbricate, and the shorter but higher velocity path lengths (as compared to gravel tracer studies) suggests that bed form spacing will be closer and will dissipate more energy compared to similar discharge and slope conditions for gravel-bed

systems. Also, this research has implications for threshold-based designs, a common river engineering approach, that use standard empirical relationships. These models will overestimate the mobility of coarse fractions for the study site, while the inverse would be true for finer grain sizes. This has implications for thresholds that are based on the assumption of an immobile channel boundary for the design discharge, but also for the design of fractional mobility cases where size selective mobility is desired for maintenance of geomorphic thresholds or habitat suitability.

4.1 Conclusions and Recommendations

A field study was undertaken using particle tracers to assess threshold and mobility characteristics of disc-shaped bed material in an incised, interbedded shale and limestone system in Toronto, Canada. The results demonstrate that the threshold of motion and transport characteristics for the study site differ from previously reported literature and empirically-based models derived from gravel-bed settings, including those typically employed in common engineering solutions.

The frequency distribution of transported particles fit a model common to other tracer-based studies (Einstein, 1937; Lamarre and Roy, 2007; Hassan and Bradley, 2015), when using a fitted two parameter gamma distribution to describe the stochastic nature of particle path lengths. Scaled transport distances for coarse particles were generally shorter than those reported in the literature. Finer particles agreed with a scaled transport model for constrained clasts, while the coarser fractions agreed with a linear fit for unconstrained clasts. Transport distance correlations to grain size were found to be statistically significant for unconstrained initial resting conditions, but not for constrained cases. These grain size based results point to increased efficacy (as compared to the literature) in reducing transport path lengths, due to some combination of particle shape and particle interactions.

Threshold conditions for different particle classes were tested using a shear exceedance model. Findings identified that many particles mobilized below critical applied bed shear having Shields ratios of less than 1.0, when assuming critical shear values based on the modified Shields diagram (Julien, 1995). Reference shear values showed a decreasing trend for dimensionless critical shear stress with increased particle size, a finding that is counter to the size selective path length results. The excess shear stress model was then used to test the field derived thresholds against shape-specific relationships for platy particles observed in laboratory settings. It was found that there is excellent agreement between the field data and that reported in the literature.

Findings of decreased size-selective path lengths, increased effect of particle interactions and threshold conditions contrast those of gravel-bed assumptions but agree with platy particles resulting in a shear

exceedance model employed to assess sediment transport characteristics. Dimensionless transport rates (τ_{*c}) analysis demonstrated grain size dependency (separation) by class, in this case with the coarser classes transporting similar rates to smaller classes. This is owing to particle hiding having a greater effect on smaller particles, as well as the effect of diminishing critical shear thresholds with increased particle size. It is therefore concluded that shorter step lengths for coarse particles don't necessarily mean a corresponding decreased in overall bedload transport rates.

Finally, a M-PM bedload transport model that was used to compare two scenarios: a) one incorporating a hiding function that normalizes based on the field-derived D_{50} threshold; and, b) one based solely on the field-based thresholds for each particle class. This method of comparison assumed the actual hiding function to be inherent within scenario b, and the results indicate a greater hiding effect for the field data than the analytical model suggests, thus supporting the diminished contribution of finer particles to the overall bedload flux (when compared to the literature). The inverse argument is also true with respect to coarse particles. The virtual velocity-based rates showed increased scatter, perhaps indicating that the periodicity of steps and rests in the study site are inherently poorly suited to this mode of analysis, or that the record of competent storms needs to be temporally expanded to lend to an interpretation of greater insight.

The relevance of sediment transport relationships to engineering applications is well known (Parker, 2006). This study identified thresholds of sediment and entrainment for different particle size classes that may be employed in several design-based settings, including as input parameters for transport modelling in similar systems. The design of target substrate sizes or bedform types required of habitat rehabilitation projects is one example, whereby the findings demonstrate that a wider range (than is predicted by the literature) of thresholds govern the incipient motion of different particle size classes, which often serve as design criteria for these types of projects (Newbury, 1993; Rosgen, 1996). Scour / deposition estimates and calculations for continuity of sediment transport calculations supporting linear infrastructure projects is also a clear application for the entrainment relationships described herein. Similarly, sediment budgeting for online impoundments within systems having similar degrees of particle angularity and implication will also benefit from these particle mobility findings.

It has been demonstrated that common engineering approaches to determining sediment mobility thresholds and transport criteria may not be adequately reflected by the conditions inherent to the bedrock controlled channels. Lithology-specific criteria such as stone type, mode of detachment, associated particle shape and bedform types should be considered when developing solutions for sediment transport problems, including channel rehabilitation design, infrastructure sizing and protection and long term

sediment budgeting. Further study is required to not only confirm the findings of this study, but also to address factors ancillary to particle transport, including antecedent particle detachment as a mechanism governing sediment supply.

Bibliography

(n.d.).

Allan, J. C., Hart, R., & Tranquili, J. V. (2006). The use of Passive Integrated Transponder (PIT) tags to trace cobble transport in a mixed sand-and-gravel beach on the high-energy Oregon Coast, USA. *International Journal of Marine Geology, Geochemistry and Geophysics, 232*, 63-86.

Andrews, E. D. (1980). Effective and Bankfull Discharges of Streams in the Yampa River Basin, Colorado and Wyoming. *Journal of Hydrology, 46*, 311-330.

Annable, W. K. (1996). *Morphological Relationships of Rural Watercourses in Southwestern Ontario and Selected Field Methods in Fluvial Geomorphology.* Peterborough: Ontario Ministry of Natural Resources.

Annable, W. K., Lounder, V. G., & Watson, C. C. (2010). Estimating Channel – Forming Discharge in Urban Watercourse is. *River Research and Applications*.

Annable, W. K., Watson, C. C., & Thompson, P. J. (2010). Quasi-Equilibrium Conditions of Urban Gravel-Bed Streams Channels in Southern Ontario, Canada. *River Research and Applications*.

Annable, W. K., Watson, C. C., & Thomson, P. J. (2012). Quasi-equilibrium conditions of urban gravel-bed stream channels in southern Ontario, Canada. *River Research and Applications, 28*(3), 302-325.

Aquartis. (2011). *Leonie System User Guide: Mobile RFID Detecbtion System (HDX 134.2 kHz).* Quebec, QC.: Aquatis Technology Ltd.

Ashida, K., & Michiue, M. (1972). Study on hydraulic resistance and bedload transport rate in alluvial streams. *Transactions, Japan Society of Civil Engineering, 206*, 59-69.

Ashworth, P., & Ferguson, R. (1989). Size-Selective Entrainment of Bed Load in Gravel Bed Streams. *Water Resources Research, 25*(4), 627-634.

AutoDesk. (2016). *AutoDesk AutoCad Map 3D User Guide.* San Rafael, California: AutoDesk Inc.

Begin, Z., Meyer, D., & Schumm, S. (1980). Knickpoint migration due to baselevel lowering. *Journal of the Waterway Port Coastal and Ocean Division*, 369-388.

Bird, J. F. (1980). Geomrphological Implications of Flood Control Measures: Lang Lang River, Victoria. *Australian Geographical Studies, 18*, 169-183.

Bledsoe, B. (2001). Linking Stormwater BMP Designs and Performance to Receiving Water Impact Mitigation. *Proceedings of an Engineering Foundation Conference*, (pp. 127 – 144). Snowmass Village, CO.

Booth, D. B. (1990). Stream-Channel incision Following Drainage-Basin Urbanization. *American Water Resources Association - Water Resources Bulletin, 26*(3), 407-417.

Booth, D. B., & Fischenich, C. J. (2015). A channel evolution model to guide sustainable urban stream restoration. *Area - by the Royal Geographical Society, 47*(4), 408-421.

Bradley, N., & Tucker, G. (2012). Measuring gravel transport and dispersion in the mountain river using passive radio tracers. *Earth Surface Processes and Landforms*, 1034 – 1045.

Brooks, A. (1988). *Channelized rivers : perspectives for environmental management.* Reading, UK: John Wiley & Sons.

Buffington, D. R. (2004). Observations on the role of lithology in strath terrace formation and bedrock channel width. *American Journal of Science, 304*, 454-476.

Buffington, J. M., Dietrich, W. E., & Kirchner, J. W. (1992). Friction Angle Measurements on a Naturally Formed Gravel Streambed. *Water Resources Research, 2*, 411-425.

Buffington, J., & Montgomery, D. (1999). Effects of hydrauulic roughness on surface textures of gravel-bed rivers. *Water Resources Research, 35*(21), 3507-3521.

Bunte, K., & Abt, S. (2001). *Sampling Surface and Subsurface Particle-Size Distributions in Wadable Gravel and Cobble Bed Streams for Analyses in Sediment Transport, Hydraulics and Streambed Monitoring.* Rocky Mountain Research Station, Forest Service. Fort Collins, CO: United States Department of Agricultural Services.

Butler, P. R. (1977). Movement of cobbles in a gravel – bed streams during a flood season. *Geological Society of America, bulletin*, 1072 – 1074.

Camenen, B., Le Coz, J., Paquier, A., & Lagouy, M. (2010). An estimation of gravel mobility over an alpine river gravel bar (Arc en Maurienne, France) using PIT-tag tracers. *Proceedings of the 5th International Conference on Fluvial Hydraulics (River Flow 2010).* Braunschweig, Germany.

Carling, P. A., Kelsey, A., & Glaister, M. S. (1992). Effect of Bed Roughness, Particle Shape and Orientation on Initial Motion Criteria. In P. Billi, C. Thorne, R. D. Hey, & P. Tacconi, *Dynamics of Gravel-bed Rivers* (pp. 23-39). Wiley & Sons.

Chiari, M., & Rickenmann, D. (2007). The Influence of Form Roughness on Modelling of Sediment Transport at Steep Slopes. *Proceedings: International Conference Erosion and Torrent Control as a Factor in Sustainable River Basin Management*, (pp. 1-8). Belgrade, Serbia.

Church, M., & Hassan, M. (1992). Size and Distance of Travel of Unconstrained Clasts on a Streambed. *Water Resources Research, 28*(1), 299 – 303.

Church, M., & Hassan, M. (2002). Mobility of bed material in Harris Creek. *Water Resources Research, 38*(11).

Coogan, A. H., & Manus, R. W. (1975). Chapter 3 - Compaction and Diagenesis of Carbonate Sands. In G. V. Chilingarian, & K. H. Wolf, *Developments in Sedimentology 18A - Compaction of Coarse-Grained Sediments, I* (pp. 79-166). New York. NY: Elsevier Scientific Publishing Company.

Copeland, R. R., McComas, D. N., Thorne, C. R., Soar, P. J., Jonas, M. M., & Fripp, J. B. (2001). *Hydraulic Design of Stream Restoration Projects.* Washington, DC: US Army Corps of Engineers.

Corporation, S. (2011). *SETX - Sokkia Classic.* Retrieved from sokkia.com: http://www.sokkia.com.sg/products/electronic/uploads/SETX.pdf

Dunne, T., & Leopold, L. (1978). *Water in Environmental Planning.* New York: W.H. Freeman and Company.

Egiazaroff, I. V. (1965). Calculation of non-uniform sediment concentrations. *Journal of Hydraulic Engineering, 91*(4), 225-248.

Einstein, H. (1937). Bedload transport as a probability problem. *Mitteilung der.*

Einstein, H. A. (1942). Formulas for the transportation of bed load. *Transactions of the American Society of Civil Engineers, 107*, 561-63.

Einstein, H. A. (1950). The bed-load function for sediment transportation in open channel flows. *United States Department of Agriculture Technical Bulletin 1026*.

Fenton, J., & Abbott, J. (1977). Initial movement of grains on a stream bed: the effect of relative protrusion. *Proceedings of the Royal Society of London A: Mathematical, Physical and Engineering Sciences, 352*(1671), 523-537.

Ferguson, R. I., & Wathen, S. J. (1998). Tracer-pebble movement along a concave river profile: Virtual velocity in relation to grain size and shear stress. *Water Resources Research, 34*(8), 2031-2038.

Folk, R., & Ward, W. (1957). Brazos River bar: a study in the significance of grain size parameters. *Journal of Sedimentary Petrology, 27*, 3-26.

Gomez, B. (1994). Effects of particle shape and mobility on stable armor develpment. *Water Resources Research, 30*, 2229-2239.

Gomez, B., & Church, M. (1989). An Assessment of Bed Load Sediment Transport Formulae for Gravel Bed Rivers. *Water Resources Research, 25*(6), 1161-1186.

Goode, J. R., & Wohl, E. (2010). Substrate controls on the longitudinal profile of bedrock channels: Implications for reach-scale roughness. *Journal of Geophysical Research, 115*, 1-14.

Goode, J., & Wohl, E. (2010). Coarse sediment transport in a bedrock channel with complex bed topography. *Water Resources Research, 46*.

Gregory, K. J., & Chin, A. (2002). Urban stream channel hazards. *Area - by the Royal Geographical Society, 34*(3), 312-321.

Habersack, H. M., & Laronne, J. B. (2002). Evaluation and Improvement of Bed Load Discharge Formulas based on Helley–Smith Sampling in an Alpine Gravel Bed River. *Journal of Hydraulic Engineering, 128*(5), 484-499.

Hammer, T. (1972). Stream and Channel Enlargement Due to Urbanization. *Water Resources Research, 8*, 1530-1540.

Harrelson, C., Rawliens, C., & Potyondy, J. (1994). *Stream Channel Reference Sites: An illustrated Guide to Field Techniques.* USDA.

Harvey, M. D., & Watson, C. C. (1986). Fluvial Processes and Morphological Thresholds in Incised Channel Restoration. *Water Resources Bulletin - American Water Resrouces Association, 22*(3), 359-368.

Haschenburger, J., & Church, M. (1998). Bed material transport estimated from the virtual velocity of sediment. *Earth Surface, Processes and Landforms, 23*, 791-808.

Hassan, M. A., Church, M., & Schick, A. P. (1991). Distance of Movement of Coarse Particles in Gravel Bed Streams. *Water Resources Research, 27*(4), 503-511.

Hassan, M. A., Smith, B. J., Hogan, D. L., Luzi, D. S., Zimmermann, A. E., & Eaton, B. C. (2008). Sediment Storage and transport in coarse bed streams: scale considerations. In H. Habersack, H. Piegay, & M. Rinaldi, *Gravel-Bed Rivers VI: From Process Understanding to River Restoration* (pp. 473-496). Elseview.

Hassan, M., & Bradley, N. (2015). Geomorphic controls on tracer particels dispersion in gravel bed rivers. *Gravel Bed Rivers 8.* Kyoto and Takayama.

Hawley, R. J. (2009). *Effects of Urbanization on the Hydrologic Regimes and Geomorphic Stability of Small Streams in Southern California.* Dissertation, Colorado State University, Fort Collins.

Hawley, R. J., & Bledsoe, B. P. (2011). How do flow peaks and durations change in suburbanizing semi-arid watershed? A Southern California Case Study. *Journal of Hydrology, 405*, 69-82.

Hjulstrom, F. (1935). Studies of morphological activity of rivers as illustrated by the rivers. *Bulletin of the Geological Institute*, 221-527.

Hollis, G. E. (1975). The Effect of Urbanization on Floods of Different Recurrence Interval. *Water Resources Research, II*(3), 431-435.

Houbrechts, G., Campenhout, J., Levecq, Y., Hallot, E., Peeters, A., & Petit, F. (2012). Comparison of methods for quantifying active layer dynamics and bed low discharge in armoured gravel – bed rivers. *Earth Surface Processes and Landforms*, 1501-1517.

Jackson, W. L., & Beschta, R. L. (1984). Influences of Increased Sand Delivery on the Morphology of Sand and Gravel Channels. *Water Resources Bulletin - American Water Resources Association, 20*(4), 527-533.

Julien, P. Y. (1995). *Erosion and Sedimentation* (2 ed.). New York, NY: Cambridge University Press.

Julien, P. Y. (2002). *River Mechanics.* New York: Cambridge University Press.

Komar, P. (1987). Selective gravel entrainment and the empirical evaluation of flow competence. *Sedimentology*, 1165-1176.

Komar, P., & Li, Z. (1986). Pivoting analysis of the selective entrainment of sediments by shape and size with application to gravel threshold. *Sedimentology, 33*, 425-436.

Krumbein, W. C. (1941). Measurement and geological significance of shape and roundness of sedimentary particles. *Journal of Sedimentary Petrology, 11*(2), 64-72.

Lamarre, H., & Roy, A. (2008). A field experiment on the development of sedimentary structures in a gravel-bed river. *Earth Surface Processes and Landforms, 33*, 1064-1081.

Lamarre, H., MacVicar, B., & Roy, A. (2005). Using Passive Integrated Transponder (PIT) Tags to Investigate Sediment Transport in Gravel-Bed Rivers. *Journal of Sedimentary Research*, 736-741.

Lane, E. W. (1955). the Importance of Fluvial Morphology in Hydraulic Engineering. *American Society of Civil Engineering, Proceedings, 81*, one – 17.

Laronne, J., & Cason, M. (1976). Interrelationships between bed morphology and bed-material transport for a small, gravel-bed channel. *Sedimentology, 23*, 67-85.

Leopold. (1968). *Hydrology for Urban Pland Planning - A guidebook on the Hydrologic Effects of Urban Land Use.* Washington: US Department of the Interior.

Leopold. (1973). River channel change with time: An example. *Geological Society of America Bulletin, 84*, 1845-1860.

Leopold. (1994). *A View of the River.* Cambridge, MA: Harvard University Press.

Leopold, L. B., & Maddock, T. (1953). *The Hydraulic Geometry of Stream Channels and Some Physiographic Implications.* Washington, DC: Geological Survey Professional Paper 252.

Li, Z., & Komar, P. (1986). Laboratory measurements of pivoting angels for applications to selective entrainment of gravel in a current. *Sedimentology, 33,* 413-423.

Liebault, F., Bellot, H., Chapuid, M., Klotz, S., & Deschatres, M. (2011). Bedload tracing in the high-sediment-load mountain stream. *Earth Surface Processes and Landforms, 37,* 385 – 399.

Lisle, T. E., & Madej, M. A. (1992). Spatial variation in armouring in a channel with high sediment supply. In P. Billi, R. D. Hey, C. R. Thorne, & P. Tacconi, *Dynamics of Gravel-Bed Rivers* (pp. 277-311). Chichester, UK: Wiley and Sons.

MacRae, C. (1993). An Alternate Design Approach for the control of Instream Erosion Potential in Urbanizing Watersheds. *Proceedings of the Sixth International Conference on Urban Storm Drainage*, (pp. 1086-1098).

MacRae, C. (1996). Experience from Morphological Research on Canadian Streams: Is Control of the Two-Year Frequency Runoff Event the Best Basis for Stream Channel Protection. *ASCE Engineering Foundaton Conference,* (pp. 144-162). Snowbird, Utah.

MacVicar, B., & Roy, A. (2011). Sediment Mobility in a forced riffle-pool. *Geomorphology,* 445-456.

MacVicar, B., Chapuis, M., Buckrell, E., & Roy, A. (2015). Assessing the Performance of In-Stream Restoration Projects Using Radio Frequency Identification (RFID) Transponders. *Water, 7,* 5560-5591.

Makin, J. H. (1948). Concept of a Graded River. *Geological Society of America Bulletin 59,* 463-511.

Meyer-Peter, E., & Muller, R. (1948). Formulas for bedload transport. *Proceedings of the 2nd meeting of the International Association of Hydraulic Structures Research,* (pp. 39-64). Stockholm, Sweeden.

Millar, R. G. (1999). Grain and form resistance in gravel-bed rivers. *Journal of Hydraulic Research, 3,* 303-312.

Montgomery, D., & Buffington, J. (1997). Channel-reach mophology in mountain drainage basins. *Geological Society of America Bulletin*, 596-611.

Newbury, R., & Gaboury, M. (1993). *Stream Analysis and Fish Habitat Design.* Winnipeg, MB: Newbury Hydraulics Ltd.

NRCS. (2007). *Stream restoration design. National Engineering Handbook. Part 654.* Washington, DC: USDA - Natural Resources Conservation Service.

Parker, G. (2006). Chapter 3 - Transport of Gravel and Sediment Mixtures. In A. S. Engineers, *Sedimentation Engineering (Manual 54)* (pp. 1-162). ASCE.

Parker, G., Klingeman, P. C., & McLean, D. L. (1982). Bedload and size distribution in paved gravel-bed streams. *Journal of the Hydraulics Division, 108*, 544-571.

Pizzuto, J. E., Hession, W. C., & McBride, M. (2000). Comparing gravel-bed rivers in paired urban and rural catchments of southeastern Pennsulvania. *Geology, 28*(1), 79-82.

Rantz, S. E. (1982). *Measurement and Computation of Streamflow: Volume 1. Measurement of stage and discharge*. Washington, DC: United States Geological Society.

Rhodes, D. (1987). The b-f-m Diagram for Downstream Hydraulic Geometry. *Geografiska Annaler. Series A, Physical Geography, 69*(1), 147-161.

Robinson, K., Hanson, G., Cook, K., & Kadavy, K. (2001). Erosion of Fractured Material. *Transactions of the ASAE, 44*, 819-823.

Rosgen, D. (1996). *Applied River Morphology* . Woldland Hydrology.

Russell, D. (1982). Controls on shale durability: the response of two Ordovician shales in the slake durability test. *Canadian Geotechnical Journal*, 1-13.

Schneider, J. M., Rickenmann, D., Turowski, J. M., Bunte, K., & Kirchner, J. W. (2015). Applicability of bed load transport models for mixed-size sediments in steep streams considering macro-roughness. *Water Resources Research, 51*, 5260-5283.

Schneider, J. M., Turowski, J. M., Rickenmann, D., Hegglin, R., Arrigo, S., Mao, L., & Kirchner, J. (2014). Scaling relationships between bed load volumes, transport distances, and stream power in steep mountain channels. *Journal of Geophysical Research: Earth Surface, 119*, 533 – 549.

Schumm, S. A. (1977). *The Fluvial System.* New York, NY: John Wiley & Sonds Inc.

Schumm, S. A., Harvey, M. D., & Watson, C. C. (1984). *Incised Channels. Morphology, Dynamics and Control*. Littleton, CO: Water Resources Publications.

Sear, D. A. (1996). Sediment transpot processes n pool-riffle sequences. *Earth Surface Processes and Landforms, 21*, 241-262.

Shields, A. (1936). Anwendung der ahnlichkeitsmechanik und turbulenz forschung auf die geschiebebewegung. *Mitteil Preuss. Versuchsanst. Wasser*.

Siddiqui, A., & Robert, A. (2010). Thresholds of erosion and sediment movement in bedrock channels. *Geomorphology, 118*, 301-313.

Simon, A. (1989). A model of channel response in disturbed alluvial channels. *Earth Surface Processes and Landforms, 14*, 11-26.

Simon, A., & Castro, J. (2003). Analysis of Processes and Forms: Water and Sediment Interactions. In G. M. Kondolf, & P. Herve, *Tools in Fluvial Geomorphology* (pp. 291-322). West Sussex, UK: John Wiley & Sons Ltd.

Simon, A., & Hupp, C. (1986). Channel evolution in modified Tennessee channels. *Procceedings, Fourth Federal Interagency Sedimentation, 2*, pp. 5-71-5-82. Las Vegas.

Sklar, L., & Dietrich, W. (2001). Sediment and rock strength controls on river incision into bedrock. *geology, 29*(12), 1087 – 1090.

Snyder, N. P., Whipple, K. X., Tucker, G. E., & Merritts, D. J. (2003). Importance of a stichastic distribution of floods and erosion thresholds in bedrocl river incision prolem. *Journal of Geophysical Research, 108*(B2), 1-15.

Soar, P. J., & Thorne, C. R. (2001). *Channel Restoration Design for Meandering Rivers.* Washington, DC: US Army Corp of Engineers.

Tinkler, K., & Wohl, E. (1988). Field Studies in Bedrock Channels. In E. Wohl, & K. Tinkler, *Rivers Over Rock: Fluvial Processes in Bedrock Channels* (pp. 261-277).

Tinkler, K., & Wohl, E. (1998). A Primer on Bedrock Channels. In R. Wohl, & K. Tinkler, *Rivers over Rock: Fluvial Processes in Bedrock Channels* (pp. 1-17). The American Geophysical Union.

Toronto, C. o. (1999). *Humber Creek Subwatershed Restoration Plan.* Toronto: The City of Toronto.

Toronto, C. o. (1999). *Humber Creek Subwatershed Restoration Plan.* Toronto: Aquafor Beech Limited.

Turowski, J. (2012). Semi-alluvial channels and sediment-flux-driven bedrock erosion. In M. Church, P. Biron,, & A. Roy, *Gravel Bed Rivers: Processes, Tools, Environments* (pp. 410-416).

Turowski, J., Hovius, N., Wilson, A., & Horng, M.-J. (2008). Hydraulic geometry, river sediment and the definition of bedrock channels. *Geomorphology, 99*, 26-38.

Turowski, J., Lague, D., & Hovius, N. (2007). Cover effect in bedroad abrasion: A new derivation and its implications for the modeling of bedrock channel morphology. *Journal of Geophysical Research, 112*, 1-16.

USACE. (2004). *HEC-RAS river analysis system - user manual.* Davis, California: U.S. Army corps of engineers. Institute for Water Resources, Hydrologic Engineering Centre.

Viles, H. (2001). Scaling issues in weathering studies. *Geomorphology, 41*, 63-72.

Wadell, H. (1935). Volume, Shape, and Roundness of Quartz Particles. *The Journal of Geology, 43*(3), 250-280.

Wathen, S. J., Ferguson, R. I., Hoey, T. B., & Werritty, A. (1995). Unequal mobility of gravel and sand in weakly bimodal river sediments. *Water Resources Research, 31*, 2087-2096.

Wathen, S. J., Hoey, T. B., & Weritty, A. (1997). Quantitative determination of the activity of within-reach sediment storage in a small gravel-bed river using transit time and response time. *Geomorphology, 20*, 113-134.

Watt, A. (1966). *Pleistocene Geology and Ground Water Resources, Township of Etobicoke.* Ontario Department of Mines.

Wentworth, C. (1922). A scale of grade and class terms for clastic sediments. *The Journal of Geology, 30*(5), 377-392.

Whipple, K. (2004). Bedrock Channels: Incision Rates and Longitudinal Profiles. *Surface Processes and Landscape Evolution*, 2-13.

Whipple, K. X., Hancock, G. S., & Anderson, R. S. (2000). River incision into bedrock: Mechanics and relative efficacy of plucking, abrasion and cavitation. *Geological Society of America Bulletin*, 1-19.

Wiele, S. M., Wilcock, P. R., & Grams, P. E. (2007). Reach-averaged sediment routing model of a canyon river. *Water Resources Research, 43*, 1-16.

Wilcock. (1997). Entrainment, Displacement and Transport of Traver Gravels. *Earth Surface Processes and Landforms, 22*, 1125-1138.

Wilcock, P. R. (1993). Critical Shear Stress of Natural Sediments. *Journal of Hydraulic Engineering, 119*(4), 491-505.

Wilcok, P. R., & Crowe, J. C. (2003). Surface-based transport model for mixed-size sediment. *Journal of Hydraulic Engineering, 129*(2), 120-128.

Willcock, P., Pitlick, J., & Cui, Y. (2009). *Sediment transport primer: estimating bed-material transport in gravel-bed rivers.* Rocky Mountain Research Station, Forest Service. Fort Collins, CO: US Department of Agriculture.

Wohl, E. (1998). Bedrock Channel Morphology in Relation to Erosional Processes. In E. Wohl, & K. Tinkler, *Rivers over Rock: Fluvial Processes in Bedrock Channels* (pp. 133-151). American Geophysical Union.

Wohl, E. (2015). Particle dynamics: The continuum of bedrock to alluvial river segments. *Geomorphology, 241*, 192-208.

Wohl, E., & Achyuthan, H. (2002). Substrate Influences on Incised-Channel Morphology. *The Journal of Geology*, 115-120.

Wohl, E., & David, G. (2008). Consistency of scaling relations among bedrock and alluvial channels. *Journal of Geophysical Research, 113*, 1 – 16.

Wohl, E., & Merritt, D. (2001). Bedrock channel morphology. *Geological Society of America Bulletin, 113*(9), 1205-1212.

Wolman. (1967). A Cycle of Sedimentation and Erosion in Urban River Systems. *Geografiska Annaler, 49*(A), 385-395.

Wolman, M. (1954). A Method of Sampling Coarse River-Bed Material. *Transactions, American Geophysical Union, 35*(6), 951-956.

Wolman, M. G., & Miller, J. P. (1960). Magnitude and Frequency of Forces in Geomorphic Processes. *The Journal of Geology, 68*(1), 54-74.

Wong, M., & Parker, G. (2006). Reanalysis and Correction of Bed-Load Relation of Meyer-Peter and Muller using their own database. *Journal of Hydraulic Engineering, 132*(11), 1159-1168.

Zingg, T. (1935). Beitrag zur Schotteranalyse. *Schweid. Min. u. Pet. Mitt., 15*, 39-140.